



(51) International Patent Classification:
G01N 33/52 (2006.01) G01N 33/80 (2006.01)
G01N 33/53 (2006.01)

(21) International Application Number:
PCT/US2012/047745

(22) International Filing Date:
20 July 2012 (20.07.2012)

(25) Filing Language: English

(26) Publication Language: English

(30) Priority Data:
61/509,776 20 July 2011 (20.07.2011) US
61/588,785 20 January 2012 (20.01.2012) US

(71) Applicants (for all designated States except US): UNIVERSITY OF WASHINGTON THROUGH ITS CENTER FOR COMMERCIALIZATION [US/US]; 4311 11th Avenue NE, Suite 500, Seattle, WA 98105-4608 (US). PUGET SOUND BLOOD CENTER [US/US]; 921 Terry Avenue, Seattle, WA 98104 (US).

(72) Inventors; and

(71) Applicants : BRAULT, Norman, D. [US/US]; 4114 Woodland Park Avenue North, Unit A, Seattle, WA 98103 (US). JIANG, Shaoyi; 14507 NE 61st Street, Redmond, WA 98052 (US).

(72) Inventors; and

(75) Inventors/Applicants (for US only): RATNER, Daniel, M. [US/US]; 5705 NE 61st Street, Seattle, WA 98115 (US). JOHNSEN, Jill, M. [US/US]; 7506 Winona Avenue North, Seattle, WA 98103 (US). KIRK, James, T. [US/US]; 923 NE 72nd Street, Seattle, WA 98115 (US). LOPEZ, Jose, A. [US/US]; 539 32nd Avenue South, Seattle, WA 98144 (US).

(74) Agent: LAWSON, L., Rhys; Christensen O'connor Johnson Kindness PLLC, 1420 Fifth Avenue, Suite 2800, Seattle, WA 98101 (US).

(81) Designated States (unless otherwise indicated, for every kind of national protection available): AE, AG, AL, AM, AO, AT, AU, AZ, BA, BB, BG, BH, BR, BW, BY, BZ, CA, CH, CL, CN, CO, CR, CU, CZ, DE, DK, DM, DO, DZ, EC, EE, EG, ES, FI, GB, GD, GE, GH, GM, GT, HN, HR, HU, ID, IL, IN, IS, JP, KE, KG, KM, KN, KP, KR, KZ, LA, LC, LK, LR, LS, LT, LU, LY, MA, MD, ME, MG, MK, MN, MW, MX, MY, MZ, NA, NG, NI, NO, NZ, OM, PE, PG, PH, PL, PT, QA, RO, RS, RU, RW, SC, SD, SE, SG, SK, SL, SM, ST, SV, SY, TH, TJ, TM, TN, TR, TT, TZ, UA, UG, US, UZ, VC, VN, ZA, ZM, ZW.

(84) Designated States (unless otherwise indicated, for every kind of regional protection available): ARIPO (BW, GH, GM, KE, LR, LS, MW, MZ, NA, RW, SD, SL, SZ, TZ,

[Continued on next page]

(54) Title: PHOTONIC BLOOD TYPING

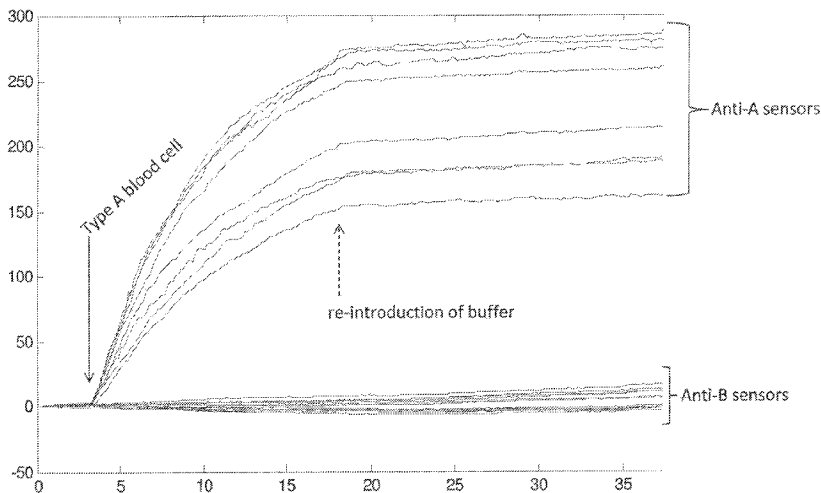


Fig.13.

(57) Abstract: Photonic devices, systems, and methods for detecting an analyte in a biological solution (e.g., whole blood) are provided. Representative photonic devices are optical ring resonators having nanoscale features and micron-sized diameters. Due to the compact size of these devices, many resonators can be disposed on a single substrate and tested simultaneously as a sample is passed over the devices. Typical analytes include blood cells, antibodies, and pathogens, as well as compounds indicative of the presence of blood cells or pathogens (e.g., serology). In certain embodiments, blood type can be determined through photonic sensing using a combination of direct detection of blood cells and serology. By combining the detection signals of multiple devices, the type of blood can be determined.



UG, ZM, ZW), Eurasian (AM, AZ, BY, KG, KZ, RU, TJ, TM), European (AL, AT, BE, BG, CH, CY, CZ, DE, DK, EE, ES, FI, FR, GB, GR, HR, HU, IE, IS, IT, LT, LU, LV, MC, MK, MT, NL, NO, PL, PT, RO, RS, SE, SI, SK, SM, TR), OAPI (BF, BJ, CF, CG, CI, CM, GA, GN, GQ, GW, ML, MR, NE, SN, TD, TG).

Published:

— *without international search report and to be republished upon receipt of that report (Rule 48.2(g))*

PHOTONIC BLOOD TYPING

CROSS-REFERENCES TO RELATED APPLICATIONS

This application claims the benefit of U.S. Provisional Application
5 No. 61/509,776, filed July 20, 2011; and U.S. Provisional Application No. 61/588,785,
filed January 20, 2012, the disclosures of which are each expressly incorporated herein by
reference in their entirety.

STATEMENT OF GOVERNMENT LICENSE RIGHTS

10 This invention was made with Government support under grant number
CBET 0930411, awarded by the National Science Foundation, and HDTRA1-10-1-0074,
awarded by the Defense Threat Reduction Agency. The Government has certain rights
in the invention.

15

BACKGROUND

Recently, there has been a surge of interest in leveraging silicon photonics for
biosensing, with the ultimate goal of producing a chip with thousands of orthogonal
sensors capable of functioning in clinical environments and available at minimal cost.
Silicon photonic biosensors have already achieved impressive sensitivities relevant for
20 biomedical applications. However, the field has been stymied by the challenge of
biological specificity, the ability to bind preferentially to an analyte of interest when
sensing in complex biological samples (e.g., blood, plasma, serum). Here we show, for
the first time on a silicon photonics platform, label-free biosensing with clinically
relevant sensitivity in undiluted human serum. Utilizing a zwitterionic polymer-based
25 surface chemistry, we dramatically limit the amount of non-specific protein adsorption to
a microring resonator in serum, while maintaining a label-free sensitivity of 10 ng ml⁻¹.
This result represents a significant step towards the practical application of silicon
photonics for medical diagnostics and the biomedical sciences.

The noteworthy potential of silicon photonics emerges from the combination of
30 excellent optical devices with control electronics to produce inexpensive integrated
photonics systems. In recent years, on-chip modulators, detectors, and hybrid lasers have
all been demonstrated. Microring resonators are exceedingly amenable to scalable
fabrication using CMOS-compatible processes, setting them apart from most other

resonant optical microcavity devices for high-throughput, multiplexed biosensing. To utilize the microring resonator for biological sensing, a binding site is chemically introduced on the surface of the sensor and a shift in the resonance wavelength of the microring is observed upon analyte binding. Exploiting this approach, SOI microring resonators have been used for the detection of a diverse range of biological species, including antibodies, proteins, nucleic acids, and bacteria, among others.

In evaluating a biosensor for a given application, there are two main figures of merit. First, the sensitivity of the device, and second, the complexity of the background solution in which the assay can be performed successfully. Many recent biosensing results have yielded excellent sensitivity, but in relatively simple solutions (low biological noise). FIGURE 1A shows the distribution of attained sensitivities, as well as the biological noise in each demonstration. The suitability of these platforms for use in clinical assays depends not only on their sensitivity, but also on the selectivity of these sensors for a particular analyte in complex biological fluids (solutions with high biological noise).

For comparison, FIGURE 1A includes the sensitivities of both colorimetric and chemiluminescent enzyme-linked immunosorbent assay (ELISA), the standard diagnostic technique used by most hospitals. Despite its widespread use and perceived effectiveness, the ELISA method is not without its limitations, as it requires signal amplification of bound analyte by primary and labeled secondary antibodies, substantially increasing both the cost and time of the diagnostic. A competing technology to ELISA, surface plasmon resonance (SPR), has also achieved low sensitivities in complex media. However, due to the complexity of plasmonic systems integration, SPR has not been realized as a highly-parallelized, portable, low-cost clinical assay. Also, while SPR is an effective label-free biosensing technology, the sensing range of SPR is limited, due to the exponential decay of the surface plasmon from the gold substrate. Thus, SPR is poorly suited to study targets, such as bacteria, where the size of the target places the majority of the refractive index change outside of the range of the evanescent wave. Therefore it would be desirable to develop a related label-free technology that could be used to sense targets at greater range from the surface of the device.

Ideally, a diagnostic test should require minimal processing of the biological sample prior to detection of the analyte of interest. However, non-specific adsorption of proteins in complex biological samples, a process known as fouling, significantly

decreases the sensitivity of label-free devices due to a lack of biological specificity at the sensor surface. Common strategies for passivating surfaces to non-specific biological interactions include adsorption of 'blocking' proteins (e.g., serum albumin) and grafting inert polymeric scaffolds (e.g., polyethylene glycol) to the surface that increase surface hydration through intermolecular hydrogen bonding. These passivation strategies are only partially effective and are inadequate to fully resist protein fouling in complex biological samples.

One biological system of great interest is the typing of blood. Immediate bloody typing is not presently enabled by any simple, portable technologies. Blood typing is necessary for personalized treatment of wounds (e.g., in combat situations) and improved safety in blood banking.

SUMMARY

This summary is provided to introduce a selection of concepts in a simplified form that are further described below in the Detailed Description. This summary is not intended to identify key features of the claimed subject matter, nor is it intended to be used as an aid in determining the scope of the claimed subject matter.

In one aspect, a photonic device for determining blood type is provided. In one embodiment, the device includes:

a sample waveguide having a sample surface; and
a binding coating covering and being in optical communication with at least a portion of the sample surface, the binding coating being configured to bind a target moiety indicative of blood type, wherein the photonic device is configured such that light passed through the sample waveguide has an evanescent field that extends a distance beyond the sample waveguide sufficient to detect the target moiety indicative of blood type.

In another aspect, a photonic system for determining a blood type is provided. In one embodiment, the system includes:

(1) a first photonic device for determining the blood type, comprising:
a first sample waveguide having a first sample surface; and

- a first binding coating covering and being in optical communication with at least a portion of the first sample surface, the first binding coating being configured to directly bind to a blood cell target moiety indicative of the blood type, wherein the blood cell target moiety is attached to a blood cell body selected from the group consisting of a blood cell, a blood cell membrane, a blood cell fragment, a microvesicle, and a blood cell-associated antigen, and wherein the first photonic device is configured such that light passed through the first sample waveguide has an evanescent field that extends a distance beyond the first sample waveguide sufficient to detect the bound blood cell target moiety; and
- (2) a second photonic device for determining blood type, comprising:
a second sample waveguide having a second sample surface; and
a second binding coating covering and being in optical communication with at least a portion of the second sample surface, the second binding coating being configured to bind to an antibody or other acellular biological species indicative of the blood type, wherein the second photonic device is configured such that light passed through the second sample waveguide has an evanescent field that extends a distance beyond the second sample waveguide sufficient to detect the antibody indicative of the blood type.

DESCRIPTION OF THE DRAWINGS

The foregoing aspects and many of the attendant advantages of this invention will become more readily appreciated as the same become better understood by reference to the following detailed description, when taken in conjunction with the accompanying drawings, wherein:

FIGURES 1A-1D. 1A: Distribution of achieved label-free sensitivities for plasmonic, mechanical, and photonic biosensors, as well as the levels of biological noise of the solutions tested. For comparison, the sensitivities of colorimetric and chemiluminescent ELISA assays are shown (dashed lines). 1B: Cross-section of the silicon with modal pattern indicated. Contours in $|E|$ are plotted in 10% increments. 1C: Illustration of the biosensor array (left) and a scanning electron micrograph of a single microring resonator (right). 1D: Schematic illustration of the operation of photonic devices in accordance with the disclosed embodiments.

FIGURE 2. Relative resonance shift for three microrings with varying surface chemistries during exposure to undiluted human plasma. As illustrated, microrings were subjected to buffer, then human plasma, and returned to buffer. The net resonance shift at the 30 minute mark and beyond is proportional to the amount of adsorbed material on the surface of the microring.

FIGURES 3A-3C. 3A: Resonance peak shifts as a function of time are shown for representative antiSA-DpC and IgGi-DpC microrings. As illustrated, sensors are initially exposed to buffer (PBS), then SA-spiked buffer ($20 \mu\text{g ml}^{-1}$), and returned to buffer. The insets illustrate the process of protein capture on the surface of the antiSA-DpC microring. 3B: Shifts in resonance as a function of increasing concentrations of SA in buffer. 3C: The relative shift difference and a best-fit Langmuir binding curve for the antiSA-DpC and IgGi-DpC microrings as a function of SA concentration.

FIGURES 4A and 4B. 4B: The resonance shift as a function of time during exposure to undiluted human serum spiked with increasing concentrations of SA. The microrings are washed briefly with buffer (PBS) between spiked serum samples. The large shift in all microrings when exposed to serum is expected due to the change in refractive index with respect to buffer. The relative shift difference is due to the specific binding of SA to antiSA-DpC sensors. 4A: A detail of the peaks of FIGURE 4B.

FIGURE 5: Protein fouling on sensors exposed to (1) a solution of fibrinogen in PBS (1 mg/ml). Microrings are returned to (2) PBS buffer to observe dissociation of non-specifically adsorbed fibrinogen. BSA-modified microrings are susceptible to fibrinogen fouling, as evidenced by a ~ 365 pm shift in the net resonance wavelength of the device. However, DpC-modified microrings are highly resistant to fibrinogen adsorption, resulting in no significant overall shift in the resonance wavelength of the microring.

FIGURE 6: Representative sensor output for antiSA and IgGi immobilization to DpC-modified microring resonators. After polymer activation (not shown), sensor baseline is achieved in immobilization buffer followed by (1) solutions of antiSA and IgGi for approximately 15 minutes, prior to a brief wash with (2) immobilization buffer. Residual, unreacted DpC chains are deactivated in (3) a high pH buffer. Microrings are exposed to (4) immobilization buffer for overall quantification of immobilized antibody.

FIGURES 7A and 7B: The relative shift difference of the microrings as a function of SA concentration in human serum for antiSA-DpC Microrings 1 (FIGURE 7A) and 2 (FIGURE 7B) follow Langmuir statistics, as expected. A best fit Langmuir binding

relation is included, yielding binding association constants of $0.027 \text{ (ng ml}^{-1}\text{)}^{-1}$ and $0.026 \text{ (ng ml}^{-1}\text{)}^{-1}$ for Microring 1 and Microring 2, respectively.

FIGURE 8: Response of antiSA-DpC Microring 2 and IgGi-DpC microrings to a second antiSA solution. After the undiluted human serum / PBS exposure steps, the microrings are exposed to (1) a solution of a second antiSA for signal amplification. Microrings are returned to (2) PBS buffer to observe bound antiSA. As expected, IgGi-DpC cannot bind the second antiSA probe, confirming that these devices did not bind SA.

FIGURE 9: Illustration of hierarchical platform with an ultra low fouling first layer and high-loading second layer.

FIGURES 10A-C: 10A: IgG functionalization levels on films with one-layer (One) and hierarchical (HA) structures prepared via SI-ATRP and SI-PIMP. 10B: Fouling levels in the presence of undiluted serum or plasma, before and after IgG functionalization. 10C: Antigen detection from PBS.

FIGURE 11: The SPR sensorgram for the fouling test in the presence of undiluted blood plasma or serum on hierarchical pCB films.

FIGURE 12: Following EDC/NHS activation, the pCB films were modified with TSH IgG, deactivated with SC buffer, and then used for TSH antigen detection.

FIGURE 13: Test data for type A red blood cells detected in solution using ring resonator photonic devices in accordance with the embodiments disclosed herein.

FIGURE 14: Test data for type B red blood cells detected in solution using ring resonator photonic devices in accordance with the embodiments disclosed herein.

FIGURE 15: Test data for type A and B antigen detected in type A plasma using ring resonator photonic devices in accordance with the embodiments disclosed herein.

FIGURE 16: Test data summary for detecting type A and B antigens in type A and B plasma using ring resonator photonic devices in accordance with the embodiments disclosed herein.

DETAILED DESCRIPTION

Photonic devices, systems, and methods for detecting an analyte in a biological solution (e.g., whole blood) are provided. Representative photonic devices are optical ring resonators having nanoscale features and micron-sized diameters. Due to the

compact size of these devices, many resonators can be disposed on a single substrate and tested simultaneously as a sample is passed over the devices. Typical analytes include blood cells, antibodies, and pathogens, as well as compounds indicative of the presence of blood cells, antibodies, or pathogens (e.g., serology). In certain embodiments, blood type or blood immune sensitization status can be determined through photonic sensing using a combination of direct detection of blood cells and serology. By combining the detection signals of multiple devices, the type of blood can be determined.

In one aspect, a photonic device for determining blood type or immune sensitization to blood type is provided. In one embodiment, the device includes:

10 a sample waveguide having a sample surface; and
 a binding coating covering and being in optical communication with at least a portion of the sample surface, the binding coating being configured to bind a target moiety indicative of blood type, wherein the photonic device is configured such that light passed through the sample waveguide has an evanescent field that extends a distance
15 beyond the sample waveguide sufficient to detect the target moiety indicative of blood type.

In one embodiment, the binding coating has a first refractive index prior to binding the target moiety indicative of blood type and a second refractive index after binding the target moiety indicative of blood type, wherein the first refractive index and the second refractive index are different, and wherein an evanescent field of electromagnetic radiation of a first wavelength extends beyond the binding coating and into any binding moiety bound to the binding coating.

FIGURE 1D illustrates a representative photonic device 100 used to capture a target moiety 111 from a biological sample fluid flowing over the device 100. The target moiety 111 is captured by a binding moiety 109 that is part of a binding coating coupled to a surface of a waveguide 105 such that the photonic device 100 is operable to detect the bound target moiety 111 by evanescent sensing via electromagnetic radiation propagating through the waveguide 105. As illustrated in FIGURE 1B, the evanescent field can extend relatively far beyond the waveguide 105, therefore the photonic device 100 allows for sensing of relatively large species (e.g., blood cells) compared with competing techniques (e.g, SPR).

The photonic device 100 includes the optical waveguide 105 disposed on a substrate 107. The device 100 is configured such that waveguiding will occur in the waveguide 105 at desired wavelengths of electromagnetic radiation. In certain embodiments, the device 100 is surrounded on three sides by the ambient environment (e.g., air) and supported by the substrate 107, as illustrated. However, it will be appreciated that cladding layers can be applied to one or more of the free surfaces of the waveguide 105 not abutting the substrate 107.

Still referring to FIGURE 1D, a binding moiety 109 is coupled to the surface of the waveguide 105. The binding moiety 109 can be directly coupled to the surface of the waveguide 105, or can be attached to an intermediate layer. Such an intermediate layer may be an anti-fouling layer, as disclosed in the Exemplary Embodiments below.

The binding moiety 109 can be any moiety known to those of skill in the art that will bind to a desired target moiety 111 contained within the sample flow. Representative binding moieties include synthetic or isolated saccharides (mono-, di-, tri-, tetra-, and oligo-) representative of the blood group antigen system, synthetic or isolated antigenic glycoconjugate (glycopeptide, glycolipid, glycosamino glycan) present on human cells and tissues, synthetic or isolated protein and peptide moieties and antigens present on human erythrocytes and other cells and tissues, lipid species specific to erythrocytes and other cells and tissues; whole or fragmented eukaryotic/prokaryotic/viral components; synthetic or modified biomimetic compounds capable of binding to carbohydrate, protein, glycoconjugate or lipid species; synthetic or isolated saccharides (mono-, di-, tri-, tetra-, and oligo-) antigens or binding moieties; antibodies, nanobodies, fab, aptamers, and other antigen-specific capture species.

Representative binding moieties are configured to bind to: blood cells, antigens, antibodies, pathogens, nucleic acids, and other biologically relevant species. In certain embodiments, the photonic device is used to determine blood type from a sample of blood in contact with the device. In such embodiments, at least one binding moiety is used to bind a target moiety is indicative of blood type. Representative target moieties include moieties similar to those listed above for the binding moieties (e.g., because both direct and indirect typing can be used). Additionally, non-antibody-based capture elements can be used instead of antibodies, as well as any binding or target moieties known to those of skill in the art.

In one embodiment, the target moiety indicative of blood type is attached to a blood cell. This approach is referred to as "direct typing", because the blood cell itself is bound to the photonic device 100 (i.e., sensed by the device) through the binding moiety 109 on the waveguide 105 coupling to the target moiety 111 that is part of the blood cell itself. Blood cells include white blood cells, red blood cells, platelets, microparticles, and portions thereof.

In other embodiments, "indirect typing" is used, wherein, the binding coating is an antigen and wherein the target moiety indicative of blood type is an antibody (e.g., through serology) indicative of immunity to blood or pathogen antigens.

While both direct and indirect typing can be used to determine blood type, these techniques can also be used to determine what blood types the blood is immunized against. Accordingly, indirect typing can be used to detect antigens that are indicative of immunity to aspects of a blood type.

Typically, only one of direct and indirect typing will be used on a single photonic device (i.e., a single resonator). This is because each device is configured to only bind to one specific target moiety. This specific binding scheme provides certainty that any binding event detected by the device will indicate the presence of the single desired target moiety. However, because photonic devices (e.g., ring resonators) can be fabricated to have such small dimensions, a single substrate ("chip" or "die") may contain up to thousands of devices, each capable of having a different binding moiety attached to its sensing surface. Therefore, on a single substrate, both direct and indirect typing may be used.

This parallel approach proves particularly powerful when undertaking the typing of blood, which may require sensing of several target moieties (e.g., blood cells and various antibodies) before the blood type can be determined accurately. Using known techniques, these multiple targets would require multiple test runs. Using the present embodiments, a single blood sample can be typed by contacting it with a single substrate containing a plurality of photonic devices having binding coatings configured such that all of the necessary target moieties will be tested for in the sample. By combining the output of the plurality of devices, the target moieties present in the blood can be determined, which, in turn, allows for determination of blood type.

The analysis of blood using both direct and indirect typing is described further below in Exemplary Embodiment 3.

While the devices disclosed have thus far been described as related to blood typing and blood immunology, it will be appreciated that the devices can also be used to determine the presence of a pathogen in a biological sample, such as blood. As with analysis of blood using the devices, the pathogen can be detected directly or indirectly by functionalizing the device with a binding moiety configured to bind to a target moiety indicative of a pathogen. The target moiety indicative of the pathogen can be one of a pathogen, a pathogen-associated antibody, a pathogen associated nucleic acid, and a pathogen-associated antigen.

10 *Binding Coatings*

All binding coatings include the binding moiety, as described above. However, the binding coating may also provide other properties. Of particular interest are coatings that improve the compatibility of the device with the sample. Because biological samples, such as blood, are of particular interest, certain coatings are antifouling, so as to decrease (or eliminate) non-specific binding.

While any antifouling coating can be used, in one embodiment, the binding coating is zwitterionic. Other antifouling coatings include hydrophilic polymer substrates (e.g. poly- and oligoethylene glycol, PEG and OEG), mono-, oligo- and polysaccharide-based non-fouling coatings, and protein-based coatings that prevent subsequent blood protein adsorption.

As disclosed in more detail in the Exemplary Embodiments below, zwitterionic films can be configured to provide antifouling properties and can be engineered to be both thin (so as to allow for evanescent detection beyond the film) and to have appropriate binding moieties on a distal surface so as to capture target moieties.

Representative zwitterionic films useful with the embodiments disclosed herein are disclosed in the following references, each of which is incorporated by reference in its entirety: U.S. Patent No. 7,879,444; U.S. Application Publication Nos. 20110195104, 20090156460, 20100099160, 20100247614, 20100249267, 20090259015, 20110097277, 20080181861, 20110282005, and 20110105712; and PCT Publication Nos. WO 2009/067562, WO 2008/083390, WO 2009/067566, WO 2009/067565, WO 2008/019381, WO 2011/057225, WO 2007/024393, WO 2011/057224, and WO 2011/057219.

In one embodiment, the binding coating comprises a poly(carboxybetaine). However, it will be appreciated that any zwitterionic material can be used as long as it meets the requirements of the devices disclosed herein.

In one embodiment, the binding coating comprises a plurality of layers, including an antifouling layer and a capture layer. As disclosed in Exemplary Embodiment 2 (and as illustrated in FIGURE 9), the antifouling coating can be engineered to have a plurality of layers, each having a separate function. In one embodiment, the antifouling layer is zwitterionic. In one embodiment, the capture layer comprises at least one binding moiety. In one embodiment, the binding moiety is configured to bind to the target moiety indicative of blood type. In certain embodiments, the binding moiety is an antigen configured to capture circulating antibody to determine indirect type. In another embodiment, the binding moiety is an immobilized antibody or similar antigen-binding moiety to determine direct type.

In one embodiment, the antifouling layer is bound to the capture layer. Multilayer binding coatings are typically covalently or ionically bound together to provide the antifouling functionality and the binding functionality. However, it will be appreciated that any means for combining these functionalities is contemplated. Furthermore, in one embodiment, the binding coating is covalently attached to the sample waveguide. Conversely, in one embodiment, the binding coating is not bound to the sample waveguide.

Photonic Devices

In one embodiment, the sample waveguide is a portion of a photonic device selected from the group consisting of a resonator and an interferometer.

In certain embodiments, the resonators are optical resonators. The optical resonator structures discussed herein can be silicon based nanostructures, and in at least one embodiment include a traveling-wave ring that is coupled to a nearby silicon waveguide. In certain embodiments, the ring resonators have a diameter of 100 microns or less. In other embodiments, the ring resonators have a diameter of 50 microns or less. In at least some embodiments the optical resonator structures employed in this technology are nano-scale. In at least some embodiments, optimized slotted waveguides use sub-100 nm features (e.g., a slot dividing the waveguide in half of 100 nm or less) to concentrate optical fields near the surface of the waveguides, to achieve relatively greater

sensitivities than can be provided by surface plasmon resonance (SPR) devices. Such slotted ring resonators and waveguide structures are known in the art.

It should be understood that while a silicon ring resonator structure is an exemplary optical cavity resonator structure that can be used as a photonic device in accordance with the embodiments disclosed herein, the concepts disclosed herein are not intended to be limited to silicon structures or ring resonator structures. The embodiments disclosed herein can be implemented on any photonic devices that can be used for evanescent wave sensing. Furthermore, such photonic can be implemented on varied substrates (not just silicon, as noted immediately above). Thus, where reference is specifically made to silicon ring resonators herein, it should be understood that such a structure is an exemplary and non-limiting embodiment.

Silicon photonics has the potential to revolutionize label-free real-time bio-sensing. Of particular interest in the present disclosure is the identification of blood type from a sample of whole blood. Through chemistries that can selectively functionalize both oxidized silicon and silicon nitride with moieties capable of selectively binding with targets (such as proteins, bacteria, and other bio-molecules), it is possible to achieve both specificity and extraordinary sensitivity in a chip-scale system based on the use of nano-photonic waveguides. The concepts disclosed herein are based on using the silicon ring resonator, which includes a traveling-wave ring that is coupled to a nearby silicon waveguide. The ring resonator structure's response is a function of the refractive index (i.e., dielectric constant) above the resonator, permitting it to sensitively and specifically detect bound species (e.g., blood cells, antigens, etc.) at or near the surface of the device. Preliminary studies indicate that such ring resonator structures possess sensitivities that exceed that of SPRs, with limits of detection low enough to detect individual small-molecule binding events.

One significance of the use of silicon nano-photonic based devices is that such silicon-based biosensors can be mass-produced with standard silicon fabrication techniques widely employed in the electronics industry, providing economies of scale enabling powerful yet inexpensive sensing devices to be achieved. As compared to SPR devices, a ring resonator device offers much greater sensitivity, potentially at lower cost, with the possibility of truly integrated data acquisition and processing offered by leveraging integrated chip technologies. By integrating optical and electronic complexity (photonic waveguides and transistors) with these sensors, it will become possible to

perform thousands of different tests, in real-time, on a single sample, with a chip that could cost a fraction of the cost of traditional biosensors in large volumes. Such a chip would have enormous impact in areas as disparate as disease diagnosis, global health, biological and chemical warfare, homeland security, home health care and diagnosis, and
5 environmental monitoring.

In certain embodiments, a single chip device is provided with photonic structures, switches, detectors, and calibration structures integrated directly onto a single die.

Silicon-on-insulator waveguides provide a remarkable platform for manipulating light on a nano-scale. Because silicon-on-insulator is a standard material for
10 manufacturing nano-scale electronic circuits, it is possible to commercially obtain material of extremely high and consistent quality, and to leverage billions of dollars of commercial nanofabrication infrastructure to build nano-scale devices. This commercial infrastructure also makes silicon an ideal platform for moving rapidly from individual devices into large-scale integrated systems. Silicon is optically transparent at
15 telecommunications wavelengths (near 1.5 μm), making the silicon waveguide a system that is inherently compatible with today's existing fiber optic infrastructure. Lastly, silicon has one of the highest refractive indices of any common dielectric material, allowing silicon waveguides to concentrate light to a remarkable degree, in particular near the surfaces of the waveguides, where the field can interact very strongly with
20 surface bound ligands as well as their targets; viruses, nucleic acids, proteins, and cells.

For evanescent wave sensing, it is extremely desirable to have very large optical fields concentrated near the surface of the optical waveguides, where binding events can occur. By concentrating an optical mode into a very small volume, it is a natural corollary that the peak electric field strength of the optical mode will increase. It is
25 possible, with integrated optics in a high index contrast system like silicon ridge waveguides, to achieve mode field concentrations that are 10,000X or more what is typically achieved for a propagating (non-focused) beam of light in air. In fact, the electric field strength of the optical mode propagating in a typical nano-scale silicon waveguide is comparable to the concentrations that can be achieved at the focus of a
30 tightly converging beam in free space. With a silicon guide, this mode can propagate for centimeters without substantial losses, whereas the focus of a lens is only microns in length. In comparing the sensitivity of a silicon photonic system to a conventional SPR biosensor solution, it is worth considering the relevant path lengths along which light

can interact with the ligand molecules. In an SPR system, the light bounces through the thin (~10 nm) layer of ligand only twice. By contrast, with ring resonators, the light will travel around an approximately 50 μm diameter ring many thousands of times on average (or more), providing a radically increased interaction length.

5 An additional advantage comes from the ability to fabricate many optical devices within the same chip, and to use lithography to align them together. As a result, there is only one alignment needed in packaging the devices; it is possible to address an entire optical system with a single fiber array connecting to the outside world. By integrating multiple devices onto the same chip, a single optical alignment can be used to address
10 hundreds or even thousands of different optical components, all of which can comprise a single complex system.

Such a system could include on-chip resonators, detectors, a switch matrix, couplers, and transistor-based control electronics. This means that once a system is in place to test and package these integrated devices, the marginal cost of adding more
15 complexity to a given device is very small.

One of the great benefits of working in the silicon-on-insulator system for photonics comes from access to cutting-edge lithographic processes. By etching an extremely narrow trench (5-100 nm) down the center of a waveguide, it becomes possible to confine a significant fraction of the propagating optical mode in the low-index slot
20 formed in the center of the guide. The divergence condition for a transverse electric mode, moreover, causes the optical field to be concentrated in the low-index region between the slots.

In certain embodiments, the silicon based ring resonator structure and fluidics components are implemented on an integrated silicon chip. A controller can be
25 implemented as a custom designed circuit (such as an application specific integrated circuit) or a microprocessor and memory, the memory including machine instructions which when executed implement a plurality of functions, including introducing a sample into the ring resonator structure, collecting optical data related to the resonance of the ring structure, and analyzing the results to determine if a particular target moiety has been
30 bound to the ring resonator structure.

In certain embodiments, fluidics components are designed to establish specific conditions in the sampling volume of the ring resonator structure to facilitate the study of the sample volume. The sample may be introduced to one or more devices using fluidics.

In such an embodiment, the fluidics components include a configurable micro-fluidic flow cell in which flow can be precisely controlled. Such fluidic components include flow cells that can be incorporated into a silicon based chip. Incorporating micro-fluidics with the photonic devices enable simplified sample delivery, routing, and analysis as related to the photonic devices.

There are many different resonator structures that can be implemented on silicon or silicon related substrates, which can achieve evanescent wave coupling effects at significantly greater distances from a sensor surface than can SPR devices. Such resonator structures, one of which is the silicone ring resonator structure discussed above, include photonic resonator crystals, photonic resonator rings, photonic resonator disks, photonic resonator linear cavities, photonic resonator racetracks, photonic distributed Bragg reflectors, and Fabry–Pérot structures. Such structures are encompassed by the term optical micro cavity resonators (or optical cavity resonators). These high-index-contrast optical cavity resonators can be implemented using silicon, silicon nitride, germanium, or any mixture thereof, in crystalline, polycrystalline and amorphous forms.

In another aspect, a photonic system for determining a blood type is provided. In one embodiment, the system includes:

- (1) a first photonic device for determining the blood type, comprising:
 - a first sample waveguide having a first sample surface; and
 - a first binding coating covering and being in optical communication with at least a portion of the first sample surface, the first binding coating being configured to directly bind to a blood cell moiety indicative of the blood type, wherein the blood cell moiety is attached to a blood cell body selected from the group consisting of a blood cell, a blood cell membrane, a blood cell fragment, a microvesicle, and a blood cell-associated antigen, and wherein the first photonic device is configured such that light passed through the first sample waveguide has an evanescent field that extends a distance beyond the first sample waveguide sufficient to detect the bound blood cell moiety; and
- (2) a second photonic device for determining blood type, comprising:
 - a second sample waveguide having a second sample surface; and
 - a second binding coating covering and being in optical communication with at least a portion of the second sample surface, the second binding coating being configured to bind to an antibody indicative of the blood type, wherein the

second photonic device is configured such that light passed through the second sample waveguide has an evanescent field that extends a distance beyond the second sample waveguide sufficient to detect the antibody indicative of the blood type.

In one embodiment, the first photonic device and the second photonic device are configured to simultaneously determine the blood type. By using simultaneous detection, the output of multiple devices can be compared to determine blood type (or detect a pathogen) in real time.

In one embodiment, the photonic system further comprises a computer configured to determine the blood type using output from both the first photonic device and the second photonic device. By comparing the response of the two different devices having two different binding coatings, a greater depth of information about the sample can be obtained using a single system. For example, both blood type (direct binding) and serology can be performed at the same time on the same sample.

In one embodiment, the photonic system further comprises a reference waveguide that does not have any binding coating. The reference waveguide may be an untreated waveguide that serves as a temperature reference that allows for calibration of the obtained data with regard to the temperature of the devices (e.g., resonators change characteristics with changing temperature and so fluctuations in temperature should be accounted for in interpreting data from devices).

In one embodiment, the photonic system further comprises a third photonic device configured to bind a moiety indicative of a pathogen. Using yet another device, a single sample can also be tested for a pathogen in order to not only characterize the blood, but also pathogens contained therein. In one embodiment, the moiety indicative of a pathogen is selected from the group consisting of a pathogen, a pathogen-associated antibody, a pathogen-associated nucleic acid, and a pathogen-associated antigen.

In additional aspects, methods for testing a biological fluid (e.g., blood) are provided. In the methods, the devices and systems provided herein are exposed to the fluid sample and the effect of the sample on the device characteristics (e.g., resonant wavelength of a ring resonator) in response to binding events on the sample surface of the device are measured. Multiple devices can be used to compare the results of multiple different binding surfaces spread across multiple devices. The testing can be simultaneous across a plurality of devices in order to facilitate real-time testing. Microfluidics can be used to deliver the sample to the devices, as well as buffer and wash

treatments. Automation can be accomplished by coordinating (e.g, by computer) the delivery of sample to the device(s) and the measurement of the output of the device(s).

Exemplary Embodiment 1. Photonic sensing in undiluted human plasma.

5 In the present study, we incorporated a novel self-adsorbing zwitterionic polymer, which is engineered to readily modify the native oxide of silicon-based devices for enhanced performance in complex biological fluids. These zwitterionic polymers, composed of carboxybetaine methacrylate (CBMA) monomers, are charge dense, yet net-neutral. This material property electrostatically induces surface hydration as opposed to
10 hydration by hydrogen bonding interactions, resulting in ultra-low protein fouling when exposed to human plasma and serum.

As demonstrated by the authors, the chemistry described herein has previously enabled the detection of biomolecules at clinically relevant sensitivities in complex media using plasmonic and mechanical sensors. Translating these zwitterionic chemistries to
15 the microring resonator opens the possibility of performing sensitive clinical assays on silicon photonics. Using this approach, we report the label-free detection of a protein at 10 ng ml^{-1} in undiluted human serum, a first in the field of silicon photonics-based biosensing.

For this study, we utilized a microring resonator chip consisting of a number of
20 individual microring sensors. The microrings are rapidly interrogated by an external laser with a center frequency of 1560 nm (approximately 250 ms per microring). Real-time peak-fitting software determines the shift in resonance wavelength of the optical cavity as a function of time. The biosensor chip is coated in a fluoropolymer cladding to minimize waveguide losses. Portions of the cladding have been removed to expose the silicon
25 oxide surface of the microring resonators for chemical modification and subsequent biosensing experimentation. The remaining fluoropolymer-clad microring resonators serve as temperature and vibration reference controls (FIGURE 1C). Mylar microfluidic gaskets are used to orthogonally address sets of microring resonators to perform chemical modifications and interrogate biological interactions at the sensor surface. The geometry
30 of the waveguide is a $500 \times 200 \text{ nm}$ ridge, as shown in FIGURE 1B, while the ring radius is $15 \text{ }\mu\text{m}$.

We introduced a self-adsorbing zwitterionic polymer DOPA-pCBMA (DpC) that dramatically reduces non-specific binding to the surface of the silicon microring.

Initially, we evaluated the ability of the DpC strategy to prevent non-specific adsorption of protein to the oxide surface on the silicon microring resonator. Microring resonator biosensors were exposed to solutions of DpC or bovine serum albumin (BSA) for surface passivation. The DpC coating was characterized by X-ray photoelectron spectroscopy (XPS) and ellipsometry. To assess the ability of the biosensor surface coatings to resist non-specific protein adsorption, we exposed DpC-modified resonators to solutions of fibrinogen (FIGURE 5) and undiluted human blood plasma (FIGURE 2). FIGURE 2 illustrates relative resonance shift for three microrings with varying surface chemistries during exposure to undiluted human plasma. As illustrated, microrings were subjected to buffer, then human plasma, and returned to buffer. The net resonance shift at the 30 minute mark and beyond is proportional to the amount of adsorbed material on the surface of the microring.

The net shift in resonance wavelength after exposure to human plasma was used to assess the amount of 'fouling' protein adsorbed to the microring resonator surface. While BSA passivation of the sensor surface decreased the amount of 'fouling' protein by around 50% compared to the 660 pm shift seen on bare silicon oxide, the DpC coating resulted in only 5 pm of shift due to fouling in undiluted human plasma. This result demonstrates the noteworthy capability of DpC coatings to yield ultra-low fouling surfaces on silicon photonic devices.

In addition to effectively eliminating sensor response to biological noise, the DpC strategy enables facile conjugation of capture ligands that can impart biological function to individual silicon microrings. When exposed to a sample solution, these capture element ligands bind target molecules generating a shift in microring resonance proportional to the target analyte concentration. We employed carbodiimide chemistries to immobilize a monoclonal antibody (antiSA) specific for the model protein analyte, streptavidin (SA). An isotype antibody (IgGi), sharing the same structure as antiSA, but with no binding specificity for SA, was immobilized to adjacent microring resonators to serve as a negative control during subsequent analyses (FIGURE 6). To demonstrate specific protein detection, phosphate-buffered saline (PBS) spiked with 20 $\mu\text{g}/\text{ml}$ SA was flowed over the microrings, shown in FIGURE 3A. In FIGURE 3A, the waveguide 105 and antiSA binding moiety 110 are used to capture SA 120. As expected, the antiSA-DpC microrings exhibited specific binding of SA, while control IgGi-DpC microrings had no significant sensor response.

Further experiments were performed to explore the relationship of SA concentration in PBS to the microring resonance shift. AntiSA-DpC and IgGi-DpC microrings were exposed to successively increasing SA-spiked PBS solutions, with intervening unspiked PBS washes, detailed in FIGURE 3B. The binding process of SA to antiSA-DpC is known to follow Langmuir statistics and the relative resonance shift difference as a function of target analyte concentration can then be expressed as:

$$d\lambda = A\alpha P / (1 + \alpha P) \quad (1)$$

Here, P is the concentration of SA in solution, α is the binding coefficient, A is a constant of proportionality depending on the number of antiSA sites, and the amount of resonance shift per SA molecule, and finally $d\lambda$ is the relative resonance shift difference. A least-squares fit of (1) to the peak shift differences between the antiSA-DpC and IgGi-DpC microrings seen in this experiment is shown in FIGURE 3C. Langmuir statistics are followed, with a best-fit binding coefficient α of $0.0034 \text{ (ng ml}^{-1}\text{)}^{-1}$. The primary goal of this study was to demonstrate the detection of analyte in undiluted serum. Undiluted human serum was spiked with SA at concentrations ranging from 10 ng ml^{-1} to $10 \mu\text{g ml}^{-1}$, encompassing a range of concentrations relevant to clinical diagnostics. Sensors were exposed to increasing concentrations of SA-spiked human blood serum, with PBS buffer washes between samples, as seen in FIGURES 4A (detail) and 4B (full scan).

The results of several functionalized microring biosensors are shown. Large resonance shifts are seen on all rings, on the order of 650 pm, due to the difference in average refractive index between PBS and human serum. A clear relative shift difference is seen between the antiSA-DpC microrings and the IgGi-DpC control microring, indicating that SA is being successfully detected. Some increase in the level of fouling is observed when compared to the unfunctionalized DpC coated microrings shown in FIGURE 2. This increase is due, in large part, to nonspecific binding of serum proteins to the immobilized antibody capture ligands. Plotting the relative peak-shift differences for the antiSA-DpC and IgGi-DpC microrings, one recovers a relationship that follows Langmuir statistics (FIGURES 7A and 7B). A least squares regression assuming relation (1) yields a binding coefficient of $0.027 \text{ (ng ml}^{-1}\text{)}^{-1}$ and $0.026 \text{ (ng ml}^{-1}\text{)}^{-1}$ for microrings 1 and 2, respectively, with the estimated number of binding sites 5.1×10^5 and 3.8×10^5 . The difference in binding sites between microrings is to be expected, as it is not possible

to precisely control the number of antibodies immobilized to the DpC scaffold on each device. Based on the approximate dimensions of the SA molecule ($5 \times 5 \times 5 \text{ nm}^3$), the observed response at saturation corresponds to 15% surface coverage of the microring in the case of antiSA-DpC Microring 1. It is worth noting that we observe a difference in the binding coefficients when characterizing antiSA-DpC/SA association in buffer versus undiluted serum. This difference in binding coefficients was anticipated due to the differences in solution composition (serum vs. buffer), and the results are comparable to what has been observed in similar biosensing experiments.

The intrinsic noise of the measurements can be estimated by the squared error between the fitted curve and the data, and is 2.8 pm and 2.5 pm RMS. Assuming a noise floor of 3σ , the functional biosensors exhibit sensitivities of approximately 10 ng ml^{-1} of SA in undiluted human serum. The achieved limit of detection is an order of magnitude more sensitive than the basic commercial colorimetric ELISA used for protein detection in clinical assays. A further control experiment utilized a second polyclonal antiSA antibody to confirm the specific capture of SA by the antiSA-DpC microrings and the absence of SA on the IgGi-DpC microring (FIGURE 8).

To leverage the high sensitivity of silicon photonic-based sensing platforms, robust chemical surface modification is imperative for label-free device performance in complex biological samples. For the first time, we have shown that label-free silicon photonic biosensors can provide ELISA-like sensitivity with extraordinary selectivity in undiluted human serum. This study highlights a rapid, simple, and versatile chemical surface modification for silicon photonic biosensors: coatings of DpC can be deposited on sensors in minutes and can be used to immobilize surface capture elements for biophotonic applications. This development in biocompatible silicon photonics represents a significant step for the application of these devices in clinical diagnostics and the biomedical sciences.

Experimental Methods

Microring resonator biosensing platform:

Silicon microring resonator biosensors and corresponding analysis instrumentation were manufactured by Genalyte, Inc. (San Diego, CA). Each biosensor chip ($6 \times 6 \text{ mm}$) consists of an array of 32 individually addressable microring resonators ($30 \mu\text{m}$ in diameter) suitable for real-time biosensing analysis. Twenty four of these

microring resonators are exposed for biosensing and eight are coated with a fluoropolymer-cladding to serve exclusively as temperature and vibration reference controls. Exposed microring resonators can be surface modified using chemistries that are compatible with the native oxide of the silicon waveguides. To minimize waveguide losses, the entire chip is coated with cladding with the exception of the exposed microring sensors, limiting all interactions with a biological sample to designated resonators. An external cavity diode laser with a center frequency of 1560 nm rapidly interrogates grating couplers of individual microring resonators (approx. 250 ms per ring), measuring the shift in resonance wavelength of the optical cavity as a function of time.

10

Materials

All chemical reagents were purchased from Sigma-Aldrich, Corp (St. Louis, MO) and used without further purification unless otherwise noted. Fraction V bovine serum albumin was purchased from EMD Chemicals (Gibbstown, NJ). Fibrinogen (Fb; Fraction I, bovine plasma) was purchased from Sigma-Aldrich. Human plasma and serum samples were provided by the Puget Sound Blood Center (Seattle, WA). Murine monoclonal antibodies against streptavidin and monoclonal immunoglobulin (IgG1) control antibodies were purchased from Abcam, Inc (San Francisco, CA). Streptavidin and polyclonal anti-streptavidin antibodies (for secondary antibody probe experiments) were purchased from Vector Laboratories (Burlingame, CA). All buffers used for biosensing experiments were prepared using ultrapure deionized water (Barnstead Nanopure; Dubuque, IA). The pH of buffer solutions was adjusted using 1M solutions of sodium hydroxide (NaOH) or hydrochloric acid (HCl). Phosphate-buffered saline (PBS, pH 7.4) was composed of 10 mM phosphate (1.9 mM KH_2PO_4 , 8.1 mM Na_2HPO_4) and 150 mM sodium chloride (NaCl). Polymer deposition was performed in deposition buffer (10 mM tris(hydroxymethyl)aminomethane (Tris), pH 8.5). Surface grafted polymer coatings were activated using freshly prepared solutions of 0.4M 1-Ethyl-3-[3-dimethylaminopropyl]carbodiimide hydrochloride (EDC) and 0.1M N-hydroxysuccinimide (NHS) purchased from Sigma-Aldrich. Antibody immobilization buffer was composed of 10 mM HEPES (4-(2-hydroxyethyl)-1-piperazineethanesulfonic acid) at pH 7.8. Silicon wafers used for XPS characterization and ellipsometry measurements were purchased from Silicon Valley Microelectronics (San Jose, CA). Hydrogen peroxide (H_2O_2) and sulfuric acid (H_2SO_4) solutions were purchased from J.T.

20
25
30

Baker (Phillipsburg, NJ) and Sigma-Aldrich, respectively. Ethanol was purchased from Deacon Laboratories (King of Prussia, PA).

Synthesis of DOPA-pCBMA (DpC) conjugates

5 The synthesis of DpC polymer conjugates has been described in detail in previous publications. Briefly, an initiator molecule was synthesized containing two adhesive catechol groups (DOPA₂; N,N'-(2-hydroxypropane-1,3-diyl)bis(3-(3,4-bis(tert-butyl)dimethylsilyloxy)phenyl)-2-(2-bromo-2-methylpropanamido)propanamide)) as described previously. Following synthesis of the CBMA monomer, DpC was
10 polymerized by atomic transfer radical polymerization (ATRP) methods overnight. DpC conjugates were purified by dialysis, resulting in a white powder. The tert-butyl)dimethylsilyloxy protecting groups were deprotected using 1M tetrabutylammonium fluoride in tetrahydrofuran (THF). The polymer was washed extensively in THF, dried under reduced pressure, and was aliquoted for storage at -20°C prior to use.

15 *Polymer Deposition on silicon microring resonator arrays:*

Prior to surface modification with DpC conjugates, microring resonator biosensor chips were vigorously cleaned to remove trace organics. Chips were exposed to freshly prepared piranha solution (1:1 30% H₂O₂: 98% H₂SO₄) for 10 minutes with mild agitation to remove bubbles that formed on the fluoropolymer-clad chip surface (*Caution!*
20 *Piranha solution is extremely dangerous as it can react explosively in the presence of organics*). Biosensor chips were washed with copious amounts of water prior to the deposition of DpC conjugates on the bare oxide surface of silicon microring resonators.

The deposition of DpC on microring resonator arrays was monitored in real-time by analyzing the change in the resonance wavelength of individual microrings over time.
25 All solutions were introduced to sensors at a flow rate of 20 µL/min using two alternating 50 µL negative-pressure syringe pumps controlled by computer software (Genalyte, Inc). Prior to deposition, deprotected DpC conjugates were diluted to a concentration of 1 mg/ml in deposition buffer (10 mM Tris-HCl; pH 8.5). The DpC solution was sonicated for 20 minutes to ensure they were fully dissolved. The biosensor chip was
30 exposed to deposition buffer to establish a signal baseline prior to introduction of the polymer solution. An array of microring resonators was exposed to the sonicated DpC solution (1 mg/ml) for 15 minutes, resulting in high-density deposition of DpC conjugates on the exposed oxide of the microring sensor surface. Microring resonators were then

washed with deposition buffer for 5 minutes, followed by an extensive wash (12 minutes) in phosphate buffered saline (PBS; pH 7.4) to remove loosely bound DpC conjugates. Finally, all sensors were exposed to deposition buffer for the quantification of DpC surface coverage by comparing the net shift in resonance wavelength to the initial sensor baseline determined in deposition buffer. As a control, a second array of microring resonators was exposed to a solution of 1 mg/ml BSA prior to performing protein fouling assays on each microring resonator biosensor chip. BSA surface functionalization was performed in parallel with DpC deposition.

Protein fouling assays using protein solutions:

The non-fouling character of DpC-coated and BSA-coated microring resonators was assessed by examining their resistance to protein fouling in simple and complex biological solutions. All solutions were flowed at 20 μ L/min and results were monitored in real-time as detailed above. After establishing a baseline in PBS, surface modified (DpC- and BSA-coated) microrings were exposed to 1mg/ml fibrinogen for 30 minutes, prior to returning to PBS for 30 minutes to assess dissociation of unbound protein (FIGURE 5). The overall shift in resonance wavelength was used to compare the amount of protein fouling for DpC- and BSA-coated sensors. The ability of the surface modified sensors to resist protein fouling in complex biological solutions was assessed using undiluted human plasma (FIGURE 2). After establishing a baseline in PBS, sensors were exposed to undiluted human plasma for 15 minutes. After returning to PBS, the overall shift in resonance wavelength was used to compare the amount of protein fouling for each surface modification strategy. The results were compared to the amount of protein fouling on unmodified (bare oxide) microring resonators following extended exposure to undiluted human plasma.

X-ray photoelectron spectroscopy (XPS) characterization of DpC polymer film:

Prior to XPS characterization of DpC films, the silicon substrate was cleaned with piranha solution, as detailed above. DpC was deposited on the silicon from a 10 mM Tris-HCl buffer for 20 minutes. The substrate was rinsed vigorously with Tris-HCl buffer, PBS, ultrapure water, then dried under a stream of nitrogen for XPS analysis. XPS composition data (Table 1) were acquired on a Kratos AXIS Ultra DLD instrument equipped with a monochromatic Al-K α X-ray source ($h\nu = 1486.6$ eV). XPS data were collected at 0 $^\circ$ takeoff angle in the hybrid mode with approximately 10 nm sampling depth, using a pass energy of 80 eV. Three spots on duplicate samples were analyzed.

Reported compositional data were averaged over multiple spots. Data analysis was performed on the *CasaXPS* software (Casa Software Ltd.). As expected, DpC modification of the native oxide of silicon decreases the percent composition of silicon (Si 2p), while increasing the percent composition of organic material (C 1s, N 1s, O 1s) at the substrate surface.

Table 1: Relative compositions of bare Si and DpC-modified Si substrates as determined by XPS; n = 3, n/d: chemical species not detected.

	Bare Si chip	DpC-modified Si chip
Si 2p	45.9 ± 2.8%	11.1 ± 0.6%
C 1s	19.9 ± 5.3%	56.1 ± 0.6%
O 1s	34.2 ± 2.5%	24.4 ± 0.8%
N 1s	n/d	2.3 ± 0.1%
Na 1s	n/d	2.8 ± 0.3%
Cl 1s	n/d	3.2 ± 0.3%
Total	100%	100%

10

Ellipsometry measurements of DpC dry film thickness:

Prior to dry film thickness characterization, the silicon substrate was exposed to solutions of DpC (1 mg/ml in 10 mM Tris-HCl) or BSA (1 mg/ml in PBS) for 30 minutes. Treated substrates were washed vigorously with their respective buffers, then ultrapure water, and dried under a stream of nitrogen. To determine the dry film thickness of DpC and BSA films on silicon, measurements were obtained using an ellipsometer (M-2000; J.A. Woollam, Inc; Lincoln, NE). The amplitude component (Ψ) and phase difference (Δ) were measured for DpC-modified and BSA-coated silicon substrates from 200-1000 nm wavelengths at varying angle of incidence (65° , 70° , 75°) at 9 spots on each chip. The data obtained from measurements was fit using a generalized Cauchy layer ($A_n = 1.45$, $B_n = 0.01$, $C_n = 0$). The thickness of the native oxide layer of the silicon substrates was determined as described above and applied to the Cauchy layer fit (~2.2nm). The average dry film thickness of DpC and BSA films on the silicon

substrates (Table 2) suggest that the polymer surface modification strategy results in very thin coatings capable of strongly resisting protein fouling.

Table 2: Ellipsometry characterization of DpC and BSA films on native oxide of Si substrates

	Average Thickness (n=9)	MSE
BSA film	3.27 ± 0.25 nm	3.16
DpC film	1.08 ± 0.10 nm	2.83

Immobilization of antibodies to DpC-modified microring resonator biosensors:

The terminal carboxylate groups of DpC-coated microring resonators were activated using carbodiimide chemistry prior to antibody immobilization. A freshly prepared activation buffer (0.4M EDC, 0.1M NHS) was passed over the DpC-modified sensors twice for 5 minutes, separated by a 1 minute wash steps with ultrapure water. Activated DpC-coatings on microrings were exposed to either monoclonal anti-streptavidin (antiSA) or immunoglobulin control antibodies (IgGi, negative control) as follows. Activated DpC-microrings were briefly exposed to immobilization buffer (10 mM HEPES, pH 7.8) to establish a baseline, followed by immediate exposure to antibody solutions (20 μ g/ml in 10 mM HEPES, pH 7.8) for 12 minutes (FIGURE 6). After antibody immobilization, the activated-DpC was quenched via hydrolysis at elevated pH (10 mM HEPES, 300 nM NaCl, pH 8.2) for 15 minutes, followed by immobilization buffer to reestablish baseline and determine the amount of immobilized antibody.

Selection criteria for functional microrings for further analysis:

Small differences in the level of immobilized antibody, as determined by the overall shift in resonance wavelength, had a significant affect on the performance of functionalized sensors. Therefore, we analyzed microring resonators that responded with 200 pm of overall resonance shift following antibody immobilization for analyte detection in undiluted human serum. We also found that high levels of antibody immobilization (>200 pm in our studies) led to a decrease in the non-fouling nature of the

DpC-coating in complex media, resulting in increased non-specific adsorption and a decreased capacity to detect analyte at low concentrations. We found that this quantitative cut-off was not required for detection of analyte in buffer for this proof-of-concept demonstration. This process emphasizes the need to fabricate and analyze arrays
5 of silicon photonic devices in order to assess the uniformity of elaborate surface modifications.

Detection of streptavidin in buffer and undiluted human serum:

The model protein streptavidin (SA) was used to demonstrate specific detection of analyte in either buffer or undiluted human serum by antibody functionalized DpC-
10 modified microring resonators. IgGi-DpC modified microrings served as a negative control for non-specific SA binding to immobilized antibodies. To demonstrate analyte detection in buffer, SA was diluted in PBS at concentrations ranging from 50 ng/ml to 10 µg/ml. After establishing a signal baseline in PBS, increasing concentrations of SA in PBS were introduced to microring resonators for 5 minutes. Concentration steps were
15 separated by 5 minute buffer (PBS) washes. The shift in resonance wavelength of antiSA-DpC microrings was compared to IgGi-DpC microrings to demonstrate specific streptavidin detection in buffer.

SA detection in undiluted serum was confirmed by exposing microring resonators to a series of SA-spiked human serum samples. To obtain sensitive device
20 measurements, undiluted SA-spiked human serum samples (10–10,000 ng/ml) were flowed over microrings for 10 minutes per sample (20 µL/min) using a negative-pressure syringe pump (Chemyx, Inc; Stafford, TX) equipped with 5mL glass syringes (Hamilton, Co; Reno, NV). Samples were separated by 5 minute buffer (PBS) washes. Specific SA binding was defined as the difference in sensor response between antiSA-DpC and IgGi-
25 DpC microrings. Functionalization of surface grafted-DpC resulted in a small increase in protein fouling compared to unmodified DpC coatings. However, there is little protein accumulation over time. Specifically, antibody functionalized DpC-modified microrings showed ~50 pm of fouling after an initial exposure to serum. However, over 60 minutes of additional exposure to undiluted serum resulted in ~55 pm of additional protein
30 fouling. These results demonstrate that DpC coatings may be functionalized with biomolecules while largely retaining their non-fouling properties during extended exposure to undiluted human serum.

Resonance Shift Calculations:

Consider a cross-section of a waveguide, expressed as $\varepsilon(x,y)$ over area Ω . It can be shown that if a portion of the waveguide cross section, Ω' , experiences a shift in dielectric constant $d\varepsilon(x,y)$, the shift in effective index (for small changes) will be:

$$5 \quad dn_{eff} = \frac{\iint_{\Omega'} |E|^2 d\varepsilon(x,y) dx dy}{2Z_0 \iint_{\Omega} \text{Re}(E^* \times H) dz dx dy} \quad (2)$$

For the experiments described in this study, two types of index shifts are relevant. First, an index shift can be created by a bulk change in the refractive index surrounding the waveguide, perhaps from switching the fluid from PBS to human serum. For the 500 x 200 nm waveguide utilized, if the cladding index is close to 1.35, the index of phosphate-buffered saline (PBS), this shift can be calculated as:

$$10 \quad dn_{eff} = 0.06 d\varepsilon_{clad} \quad (3)$$

Another type of index shift is caused by a molecule becoming bound to the surface of the microring. In this case, the integral in (2) should be taken over the entire area into which the molecule might bind, call this Ω' , and then the result discounted by 15 A/Ω' , where A is the cross-sectional area of the molecule. The molecules under investigation in this work have typical sizes ranging from 5 to 15 nm. The hydrated DpC layer is also estimated to be on the order of 10 nm. Therefore all index shifts occur within 30 nm of the surface of the waveguide. The optical fields exhibit minimal falloff over such a short distance, rendering the index shift independent to small changes in 20 positioning of the molecules. Once the index shift is known, it is easy to calculate the shift in resonance wavelength:

$$d\lambda = \lambda \frac{dn_{eff}}{n_g} \quad (4)$$

Here n_g is the group index of the waveguide, 4.05 near 1550 nm. The waveguide effective index is 2.33. For a molecule, (4) would need to be multiplied by L'/L , the length of the molecule, divided by the circumference of the microring, in this case 94 μm . Combining all these expressions, we have:

$$5 \quad d\lambda = \left(\frac{\lambda}{n_g L} \right) \left(\frac{\frac{1}{\Omega' \iint_{\Omega} |E|^2 dx dy}}{2Z_0 \iint_{\Omega} \text{Re}(E^* \times H) dz dx dy} \right) \frac{m}{\rho} (\varepsilon_{\text{molecule}} - \varepsilon_{\text{background}}) \quad (5)$$

Here m is the total mass of bound molecules, ρ is the density of the molecule, and $\varepsilon_{\text{molecule}}$ and $\varepsilon_{\text{background}}$ are the dielectric constants of the molecule and background materials, respectively. We have due to numerical calculation:

$$\left(\frac{\frac{1}{\Omega' \iint_{\Omega} |E|^2 dx dy}}{2Z_0 \iint_{\Omega} \text{Re}(E^* \times H) dz dx dy} \right) = 0.93 \frac{1}{\mu\text{m}^2} \quad (6)$$

10

Also:

$$\left(\frac{\lambda}{n_g L} \right) = 0.0041 \quad (7)$$

We can now calculate the index shift per binding event, or equivalently, the total mass bound, for a molecule where we know the refractive index and density. As noted in
15 the main paper, there is a simple linear relation between the bound mass and the wavelength shift of a resonance peak. Streptavidin (SA) and antiSA should have approximate refractive index 1.45, density 1.35 g/ml, and respective molecular weights of 60, 150 kDa. We note that the approximately 600 pm resonance shift seen in the human serum experiments suggests that the index of human serum is 1.36. The shifts predicted
20 in (4) should then be nearly identical for a given bound molecule, regardless of whether the background is PBS or human serum. We have, finally, 7.86×10^{-5} pm of shift per SA

binding event in PBS. This can also be expressed as a mass sensitivity; 0.79 pm/fg of resonance shift is expected, in agreement with the 0.89 pm/fg measured elsewhere for a similar system. The number of SA binding sites for a given peak resonance shift difference can then be readily calculated.

5 *Confirmation of specific streptavidin binding to antiSA-DpC microrings:*

To confirm specific SA binding to antiSA-DpC microrings, a polyclonal antiSA antibody (50 µg/ml) was flowed over sensors after detection of SA in serum. By analyzing the formation of an antibody "sandwich" (antiSA/SA/antiSA-DpC), we were able to determine if there was specific capture of SA by the antiSA-DpC sensors. The antiSA-DpC microrings exhibited a significant peak shift, while the IgGi-DpC control microring showed no shift (FIGURES 7A and 7B). This suggests that the bound SA on the antiSA-DpC microring was able to bind the polyclonal antiSA antibodies as expected, while simultaneously confirming a lack of SA bound to the IgGi-DpC microring. The net peak shift, approximately 100 pm, was around a factor of 3 larger than the final relative peak shift of the antiSA and IgGi microrings, which was approximately 30 pm. This is as expected, due to the relative molecular weights of 60 and 150 kDa for SA and antiSA respectively. Further, this result indicates an approximate 1:1 correspondence between the final number of SA molecules bound, and the final number of polyclonal antiSA antibodies bound from solution.

20

Exemplary Embodiment 2. Hierarchical anti-fouling layer for photonic sensing.

Surface chemistries for biosensors, implantable medical devices targeted drug/gene delivery carriers, tissue scaffolds, and targeted molecular imaging probes in complex media remain a great challenge due to high nonspecific adsorption and low binding capacity of molecular recognition elements. Currently, few materials have been developed to reduce nonspecific protein adsorption, including poly(ethylene glycol) (PEG), mannitol tetraglyme, and zwitterionic polymers. The effectiveness of protein resistant materials relies on their high surface packing densities. Unfortunately, highly dense two-dimensional (2D) polymer films elicit the limitation of a low ligand-binding capacity. At the same time, a three-dimensional (3D) carboxymethylated dextran-based hydrogel binding matrix was previously developed, enabling very high protein loading due to an open polymer structure. However, this open structure only provides weak surface resistance to nonspecific protein adsorption, particularly in complex media such

30

as blood. New polymers with precisely controlled architecture are desirable for exploring novel structure-property correlations and achieving unique properties for many applications. In this communication, we propose a unique strategy of developing hierarchical polymer films with structurally regulated functionalities through integrating 2D and 3D structures so as to achieve ultra low nonspecific binding and high loading of molecular recognition elements.

Our first attempt to construct a binding platform with a hierarchical architecture was demonstrated with two distinct surface-initiated techniques. These "grafting from" approaches, based on controlled "living" radical polymerizations, were particularly promising for the preparation of polymer brushes as they permit precise control over chemical composition, film thickness, and architecture. As shown in Scheme 1, the films were prepared via surface initiated atom transfer radical polymerization (SI-ATRP) and surface initiated photoiniferter-mediated polymerization (SI-PIMP). The first layer was grown in a controlled manner to reach a high surface packing density. The second layer, with a low surface packing density, was achieved through "termination" or "regeneration" of the living capped species at the polymer chain end for SI-ATRP and SI-PIMP, respectively.

Due to the dual functionality of poly(carboxybetaine) (pCB) films, a proof-of-concept experiment was performed with zwitterionic pCB using a surface plasmon resonance (SPR) biosensor for demonstrating the novel hierarchical architecture. Previous reports of surface-tethered pCB brushes formed by both SI-ATRP and SI-PIMP have achieved excellent resistance to nonspecific protein adsorption in the presence of complex media, such undiluted human blood serum and plasma, to fouling levels below 5 ng cm⁻². These fouling levels can be maintained following the immobilization of around 250 ng cm⁻² of antibody using conventional 1-ethyl-3-(3-dimethylaminopropyl)-carbodiimide and N-hydroxysuccinimide (EDC/NHS) coupling chemistry under biologically friendly conditions. However, this functionalization level only corresponds to an IgG monolayer. Herein, pCB-based platforms with hierarchical structures on a SPR sensor surface are presented for the sensitive quantification of IgG immobilization, antigen binding, and nonspecific protein adsorption.

As shown in FIGURE 9, ATRP was combined with a "termination" approach for demonstrating the novel architecture. ATRP involves a dynamic equilibrium between activated propagating radicals and dormant halide end-capped polymer chains, yielding

low polydispersity and controlled growth. This "living" characteristic enables re-initiation from macroinitiators for the synthesis of block copolymers. In order to achieve hierarchical pCB films possessing ultra low fouling and high loading properties via SI-ATRP, a densely packed first layer was grown from a gold coated SRP chip modified with an alkyl bromide terminated self-assembled monolayer (SAM). The chips were then submerged in a methanolic solution containing 2,2' bi-pyridine, CuBr, and CB monomer under nitrogen protection and allowed to react overnight. The resulting thickness was 7.6 ± 0.3 nm (Table 3). Importantly, these conditions enabled a highly dense yet thin film to be grown. While the high density is key for achieving low fouling, a thin film is desired for many sensing applications, such as SPR, as the signal intensity/sensitivity decays exponentially from surface of the metal substrate. To establish a hierarchically structured pCB film for increasing the binding capacity, the macroinitiator density for re-growth of the second pCB layer was regulated via azide substitution of bromide species thus "terminating" the future growth of the corresponding chains during the second ATRP reaction. The density of the polymer chains can be controlled by the azide concentration and reaction time. In this study, a 2 hr submersion using an azide concentration of 0.1 M produced the optimal second layer polymer density for protein immobilization. For the growth of the second pCB layer, water-accelerated polymerization with a solvent consisting of 50% water in methanol was employed to induce a high polydispersity of polymer chains. The resulting thickness of the structured film with azide substitution was higher than that without treatment. This is in agreement with previous reports showing rapid bimolecular termination at high initiator densities using aqueous ATRP whereas more dilute initiators enabled continued linear and controlled polymer growth.

Table 3. Thickness of films prepared via SI-ATRP and SI-PIMP with and without treatment to capped species.

	<u>SI-ATRP</u>	<u>SI-PIMP</u>
	Thickness (nm)	Thickness (nm)
First Layer	7.6 ± 0.3	10.8 ± 0.8
Re-growth (without treatment)	13.2 ± 0.3	32.1 ± 0.6
Re-growth (with treatment)	17.5 ± 0.9	46.1 ± 1.6

In contrast to SI-ATRP, SI-PIMP is apt to release capped species from the polymer chains during polymerization, primarily due to bimolecular termination. This irreversible termination significantly hampers future polymer growth. Therefore, in order to control the chain density of the second layer via SI-PIMP, a "regeneration" approach was adopted in which the addition of a deactivator, tetraethylthiuram disulfide (TED), was able to preserve the end-capped photoiniferter groups on the grafted polymers for re-growth of the second layer with controlled grafting density. SPR gold substrates were first modified with the photoiniferter (N,N-(Diethylamino)-dithiocarbamoylbenzyl(trimethoxy)-thiol (DTCA)) to form SAMs. Similarly to SI-ATRP, the first layer for SI-PIMP was also synthesized in 100% methanol to form a highly dense and thin film. Reactions were conducted using a 30 min UV irradiation and the resulting film thicknesses are shown in Table 3. The first layer thicknesses prepared with 2 μM TED was comparable to that without TED (11.1 ± 0.6 nm). Subsequently, the films were re-initiated in a 90% water/methanol solution resulting in TED treated films with greater thicknesses than those made without, reflecting the ability of TED for preserving the reactive photoiniferter end groups and thereby maintaining the "living" characteristic of SI-PIMP.

In this study, functionalization and fouling tests were monitored in situ using a custom-built SPR sensor with wavelength modulation. For antibody immobilization, the films were activated using EDC/NHS coupling chemistry followed by injecting an anti-human thyroid stimulating hormone (anti-TSH) IgG solution. The unreacted NHS esters were then hydrolyzed back into the original carboxylate groups using 10 mM sodium carbonate buffer with 300 mM NaCl at pH 10. As shown in FIGURE 10A, the functionalization levels were estimated as 195.9 ng cm^{-2} and 417.0 ng cm^{-2} for one-layer ("One" in FIGURES 10A-10C) and hierarchical ("HA" in FIGURES 10A-10C) films prepared via SI-ATRP; 253.0 ± 14.8 and $792.7 \pm 54.7 \text{ ng cm}^{-2}$ for one-layer and hierarchical films from SI-PIMP. Here, an increase in binding capacities for IgG molecules on pCB films was observed for the hierarchical architecture. For the IgG functionalized one-layer films, the binding capacities were similar to that obtained with carboxyl-terminated SAMs. Although pCB provides abundant carboxyl groups for biomolecule conjugation, highly-packed polymer brushes hamper the penetration of

molecules due to steric hindrance and therefore modification only takes place at the accessible functional groups on the topmost layer of the pCB films. However, for the hierarchical films, the chain densities of the second layer were controlled via the termination and regeneration approaches. Constructed from highly dense first layers, the loose second layers allowed diffusion of antibodies thus enabling conjugation with NHS esters throughout the entire second layer. The control experiments using the structured films without treatment of capped species were also conducted. IgG immobilization levels were reduced by 30% and 64% for SI-ATRP and SI-PIMP, respectively, compared to the corresponding treated hierarchical pCB films. This evidence indicates that a sufficient number of accessible binding groups for protein modification, made apparent by the larger second-layer film thicknesses of the treated films, are a determining factor of the ligand loading capacity.

FIGURE 11 is an SPR sensorgram for the fouling test in the presence of undiluted blood plasma or serum on hierarchical pCB films. FIGURE 12 is an SPR sensorgram following EDC/NHS activation, the pCB films were modified with TSH IgG, deactivated with SC buffer, and then used for TSH antigen detection.

The protein fouling levels on one-layer films and hierarchical pCB films before and after IgG functionalization were tested by flowing undiluted blood serum or plasma (FIGURE 10B). All fouling levels were very low as a result of the highly-packed first pCB layers serving as ultra low fouling backgrounds. As a comparison, the fouling level for a loose pCB one-layer film with a thickness of 12.3 nm prepared from 50% water in methanol by SI-PIMP was as high as 54.3 ng cm^{-2} in the presence of serum. These results indicate that the high performance of pCB for effective resistance against non-specific adsorption and high ligand loading is established on the basis of control over the polymer architecture.

Solutions containing TSH antigen were flowed over the functionalized surfaces to evaluate the antigen detection ability (FIGURE 10C) and the bio-activities (molar ratios of antigen to antibody) of the binding platforms. TSH binding capacities were $42.1 \pm 2.4 \text{ ng cm}^{-2}$ and $128.5 \pm 26.2 \text{ ng cm}^{-2}$ for one-layer and hierarchical pCB films from SI-PIMP, respectively. The corresponding bio-activities were 0.89 and 0.87. The one-layer and hierarchical pCB films made via SI-ATRP bound 30.4 ng cm^{-2} and 74.7 ng cm^{-2} of TSH, respectively, with bio-activities of 0.80 and 0.93. Thus, this study demonstrates that the binding capacity for antigens is well correlated to the degree of

antibody immobilization and that the bio-activity of the film is not affected by the pCB hierarchical architecture.

In conclusion, new methodologies were developed for creating surface-initiated polymer brushes with hierarchical architectures possessing distinctive structurally regulated functionalities. Through combining the benefits of 2D and 3D polymer structures, a unique binding platform with ultra low fouling and high loading was established to serve as a new model for advancing surface chemistry needs. While this work was demonstrated with pCB prepared via the "grafting from" approach using a SPR biosensor, this is a powerful and yet generic concept which can be applied to other surface chemistries, such as dextran or PEG-based materials, and is easily adaptable to other sensing platforms and devices. Furthermore, the preparation method for the hierarchical architecture can be modified for other applications, such as "click" or thiol-ene "grafting to" chemistries. This research illustrates the great promise of this hierarchical surface coating development for multi-functional surface chemistry in biotechnological and nano-engineering applications.

Experimental Methods

pCB films via SI-ATRP

Mercaptoundecyl bromoisobutyrate (SI-ATRP initiator) and carboxybetaine acrylamide (CB) monomer were synthesized as described previously. SAMs on cleaned SPR chips of ATRP initiator were formed by soaking overnight in ethanol (0.1 mM). Upon removal, the chips were rinsed with ethanol, THF, ethanol, and then dried and placed in a custom glass tube reactor under nitrogen. In a separate glass tube, CuBr (8.86 mg), 2,2'-bipyridine (57.85 mg), and CB (600 mg) were added and placed under nitrogen. The solids were dissolved in nitrogen purged methanol (4 mL) and transferred to the chips and reacted for 24 hours at 25°C in a shaker bath. For single layer films, the chips were rinsed with water and stored overnight in PBS. For hierarchical films, the solution was quenched with CuBr₂ (275.87 mg) in methanol (4 mL) and then rinsed with methanol, water, and submerged in PBS. The second block was then grown via repeating the above procedure but using a nitrogen purged methanol:water (1:1) and reacting for 3 hours. Termination of bromine groups and replacement with non-reactive azide moieties for reducing the second block polymer density was achieved by submerging the single

layer chips in an aqueous azide solution (0.1 M) for 2 hours, removing and rinsing with PBS, water, and then drying for ATRP.

pCB films via SI-PIMP

5 The DTCA photoiniferter was synthesized as described previously. SAMs on cleaned SPR chips of the photoiniferter were formed by soaking overnight in THF containing DTCA (2 mM) followed by rinsing with THF and drying with a stream of air. For single layers, the photoiniferter modified chip was transferred to a quartz reaction tube along with 170 mg of CB monomer and placed under nitrogen. Nitrogen purged
10 methanol (5 mL) containing TED (2 μ M) was transferred to the reaction tube. The photo-polymerization was then conducted for 30 min using a UV lamp (302 nm) coupled with a 280 nm cutoff filter for preventing deterioration of thiol-gold bonds. Following the reaction, the chips were removed and rinsed with water, PBS, and then submerged in PBS. For the hierarchical films, the single layer film was re-initiated using the identical
15 procedure except for the using nitrogen purged methanol:water (10:90) in the absence of TED.

Ellipsometry

20 The thickness of the pCB films were determined using an ellipsometer (Model alpha-SE, J.A. Woollam, Lincoln, NE) using the 380 – 900 nm wavelength range at an incidence angle of 70°. The results were fitted to a Cauchy module.

Non-specific Protein Adsorption, Antibody Modification, and Antigen Detection

25 The non-specific adsorption, antibody immobilization, and antigen detection was monitored using a custom-built four-channel SPR sensor with the Kretschmann configuration and wavelength modulation as described previously. SPR chips were made of a glass slide coated with titanium (2 nm) followed by gold (48 nm) using an electron beam evaporator. A 1 nm SPR wavelength shift corresponded to a change in the protein surface coverage of 17 ng cm⁻² which was corrected to account for loss of sensitivity due
30 to the polymer films using previously described methods. For fouling experiments, undiluted human serum or plasma were injected (10 min, 40 μ L min⁻¹) and the wavelength shift between PBS baselines was converted to a surface coverage. Anti-TSH was immobilized by first injecting 10 mM sodium acetate (SA, pH 5) followed by

EDC/NHS (0.2 M/0.05 M in water) for 7 min at 30 $\mu\text{L min}^{-1}$. Anti-TSH (50 $\mu\text{g mL}^{-1}$ in 10 mM HEPES pH 7.5) was injected (20 min, 20 $\mu\text{L min}^{-1}$) followed by deactivating with 10 mM sodium carbonate containing 300 mM sodium chloride (pH 10) for 10 min and the SA both at 30 $\mu\text{L min}^{-1}$. Immobilization was calculated as the difference between SA
5 baselines before IgG injection and after deactivation. TSH was antigen binding was then monitored by first injecting PBS and then antigen (1 $\mu\text{g mL}^{-1}$ in PBS at 40 $\mu\text{L min}^{-1}$) following by PBS.

Materials

10 Copper (I) Bromide (99.999%), 2,2'-bipyridine (BPY, 99%), tetrahydrofuran (THF), Tetraethylthiuram disulfide (TED), methanol, 4-(2-hydroxyethyl)-1-piperazineethanesulfonic acid (HEPES), and phosphate buffered saline (PBS, 0.01 M phosphate, 0.138 M sodium chloride, 0.0027 M potassium chloride, pH 7.4) were purchased from Sigma-Aldrich (St. Louis, MO). Ethanol (200 Proof) was purchased
15 from Decon Laboratories (King of Prussia, PA). Sodium carbonate anhydrous was purchased from EMD Chemicals (Darmstadt, Germany). Sodium chloride (NaCl) and ether were purchased from J.T. Baker (Phillipsburg, NJ). Sodium acetate anhydrous was purchased from Fluka (subsidiary of Sigma Aldrich, St. Louis, MO). 1-Ethyl-3-(3-dimethylaminopropyl) carbodiimide hydrochloride (EDC) and N-hydroxysuccinimide
20 (NHS) were purchased from Acros Organics (Geel, Belgium). Pooled human serum was purchased from Biochemed Services (Winchester, VA). Antibody to thyroid stimulating hormone (anti-TSH) and the TSH antigen were purchased from ThermoFisher Scientific (Waltham, MA). Water used in the experiments was purified using a Millipore water purification system with a minimum resistivity of 18.2 $\text{M}\Omega\text{ cm}$.

25

Exemplary Embodiment 3. Blood typing

Direct Typing

To prepare biosensor chips for direct red blood cell (RBC) typing assays,
30 microring resonator arrays were coated with adsorbed Protein A. After briefly washing the chip, monoclonal anti-blood group IgG antibodies (anti-A and anti-B) as well as a negative control monoclonal IgG (antiPSA) were microspotted on separate regions of each chip. The entire biosensor chip was blocked with bovine serum albumin to minimize

non-specific adsorption of red blood cell fragments. The membranes of red blood cells (Type A or Type B RBCs) were ruptured by resuspending cells in a hypotonic lysis buffer, and cell fragments were washed via centrifugation to remove expelled cellular contents including hemoglobin from solution. Ruptured red blood cells were diluted in phosphate-buffered saline and introduced to functionalized sensor arrays at a flow rate of 20 μ l/min for 15 minutes. The sensor responses of anti-A and anti-B functionalized microring resonators were normalized to the response of the negative control antiPSA sensors. The results of a plurality of anti-A and anti-B sensors are presented in FIGURE 13 (testing for Type A RBC) and FIGURE 14 (testing for Type B RBC). The specific detection of both Type A and Type B RBC is apparent from the disclosed data.

Indirect Typing

Arrays of microring resonators were coated with the non-fouling DpC zwitterionic polymer as previously described herein. Surface grafted-DpC polymer chains were chemically modified to covalently immobilize the streptavidin (SA) protein for further derivatization of the sensors with biotinylated capture elements. SA-DpC microrings were microspotted with biotinylated blood group antigens (A and B antigens) for specific capture of anti-blood group antibodies from human sera. Functionalized sensor arrays were then exposed to undiluted human plasma (Type A or Type B plasma), and the differential sensor response was compared to determine the presence of anti-blood group antibodies in blood samples. The testing of sensors exposed to type A plasma is illustrated in FIGURE 15. A summary of test data from multiple sensors exposed to both type A and type B plasma is illustrated in FIGURE 16. The consistency of the results presented in FIGURES 15 and 16 demonstrate the usefulness of the photonic devices to determine blood type.

While illustrative embodiments have been illustrated and described, it will be appreciated that various changes can be made therein without departing from the spirit and scope of the invention.

30

CLAIMS

The embodiments of the invention in which an exclusive property or privilege is claimed are defined as follows:

1. A photonic device for determining blood type or immune sensitization to blood type, comprising:

a sample waveguide having a sample surface; and

a binding coating covering and being in optical communication with at least a portion of the sample surface, the binding coating being configured to bind a target moiety indicative of blood type or immune sensitization to blood type, wherein the photonic device is configured such that light passed through the sample waveguide has an evanescent field that extends a distance beyond the sample waveguide sufficient to detect the target moiety indicative of blood type.

2. The photonic device of Claim 1, wherein the target moiety indicative of blood type is attached to a blood cell.

3. The photonic device of Claim 2, wherein the blood cell is selected from the group consisting of a white blood cell, a red blood cell, a platelet, and a microparticle.

4. The photonic device of Claim 1, wherein the binding coating is an antigen and wherein the target moiety indicative of blood type is an antibody indicative of blood or pathogen antigens.

5. The photonic device of Claim 1, wherein the binding coating is antifouling.

6. The photonic device of Claim 1, wherein the binding coating is zwitterionic.

7. The photonic device of Claim 6, wherein the binding coating comprises a poly(carboxybetaine).

8. The photonic device of Claim 1, wherein the binding coating comprises a plurality of layers, including an antifouling layer and a capture layer.

9. The photonic device of Claim 8, wherein the antifouling layer is zwitterionic.

10. The photonic device of Claim 8, wherein the capture layer comprises at least one binding moiety.

11. The photonic device of Claim 10, wherein the binding moiety is configured to bind to the target moiety indicative of blood type.

12. The photonic device of Claim 8, wherein the antifouling layer is bound to the capture layer.

13. The photonic device of Claim 1, wherein the binding coating is covalently attached to the sample waveguide.

14. The photonic device of Claim 1, wherein the binding coating is not bound to the sample waveguide.

15. The photonic device of Claim 1, wherein the binding coating has a first refractive index prior to binding the target moiety indicative of blood type and a second refractive index after binding the target moiety indicative of blood type, wherein the first refractive index and the second refractive index are different, and wherein an evanescent field of electromagnetic radiation of a first wavelength extends beyond the binding coating and into any binding moiety bound to the binding coating.

16. The photonic device of Claim 1, wherein the sample waveguide is a portion of a photonic device selected from the group consisting of a resonator and an interferometer.

17. The photonic device of Claim 1, wherein the sample waveguide is a portion of a photonic device selected from the group consisting of a ring resonator, a Bragg reflector, and a Mach-Zehnder interferometer.

18. A photonic system for determining a blood type, comprising:
- (1) a first photonic device for determining the blood type, comprising:
 - a first sample waveguide having a first sample surface; and

a first binding coating covering and being in optical communication with at least a portion of the first sample surface, the first binding coating being configured to directly bind to a blood cell target moiety indicative of the blood type, wherein the blood cell target moiety is attached to a blood cell body selected from the group consisting of a blood cell, a blood cell membrane, a blood cell fragment, a microvesicle, and a blood cell-associated antigen, and wherein the first photonic device is configured such that light passed through the first sample waveguide has an evanescent field that extends a distance beyond the first sample waveguide sufficient to detect the bound blood cell target moiety; and

(2) a second photonic device for determining blood type, comprising:
a second sample waveguide having a second sample surface; and
a second binding coating covering and being in optical communication with at least a portion of the second sample surface, the second binding coating being configured to bind to an antibody indicative of the blood type, wherein the second photonic device is configured such that light passed through the second sample waveguide has an evanescent field that extends a distance beyond the second sample waveguide sufficient to detect the antibody indicative of the blood type.

19. The photonic system of Claim 18, wherein the first photonic device and the second photonic device are configured to simultaneously determine the blood type.

20. The photonic system of Claim 18, further comprising a computer configured to determine the blood type using output from both the first photonic device and the second photonic device.

21. The photonic system of Claim 18, further comprising a reference waveguide that does not have any binding coating.

22. The photonic system of Claim 18, further comprising a third photonic device configured to bind a target moiety indicative of a pathogen.

23. The photonic system of Claim 22, wherein the target moiety indicative of a pathogen is selected from the group consisting of a pathogen, a pathogen-associated antibody, a pathogen-associated nucleic acid, and a pathogen-associated antigen.

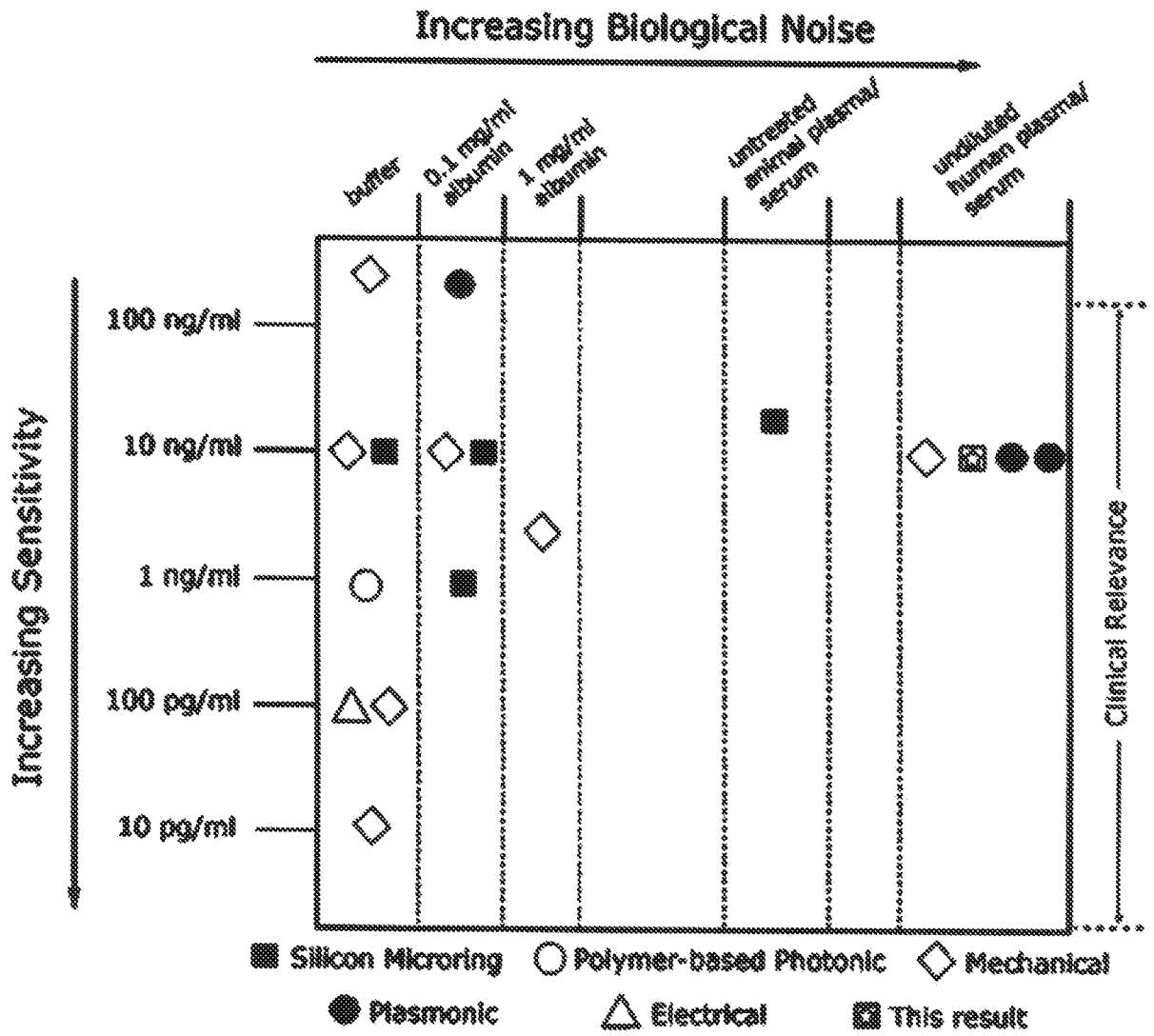


Fig. 1A.

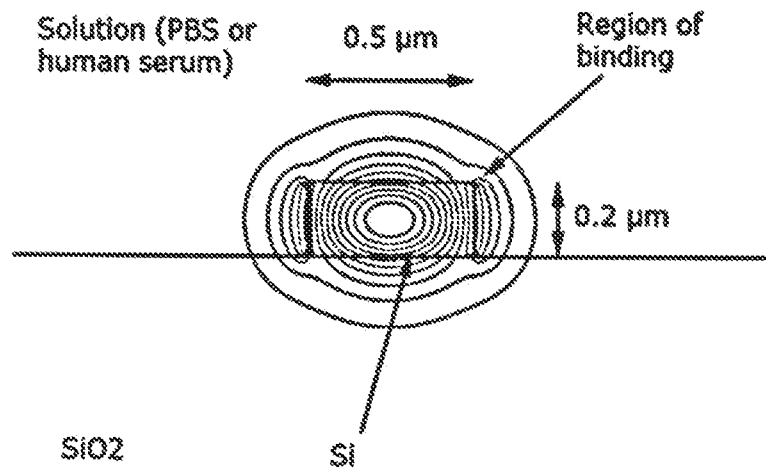


Fig. 1B.

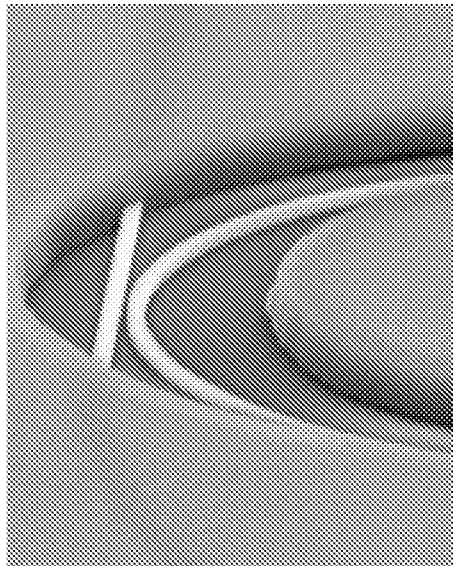
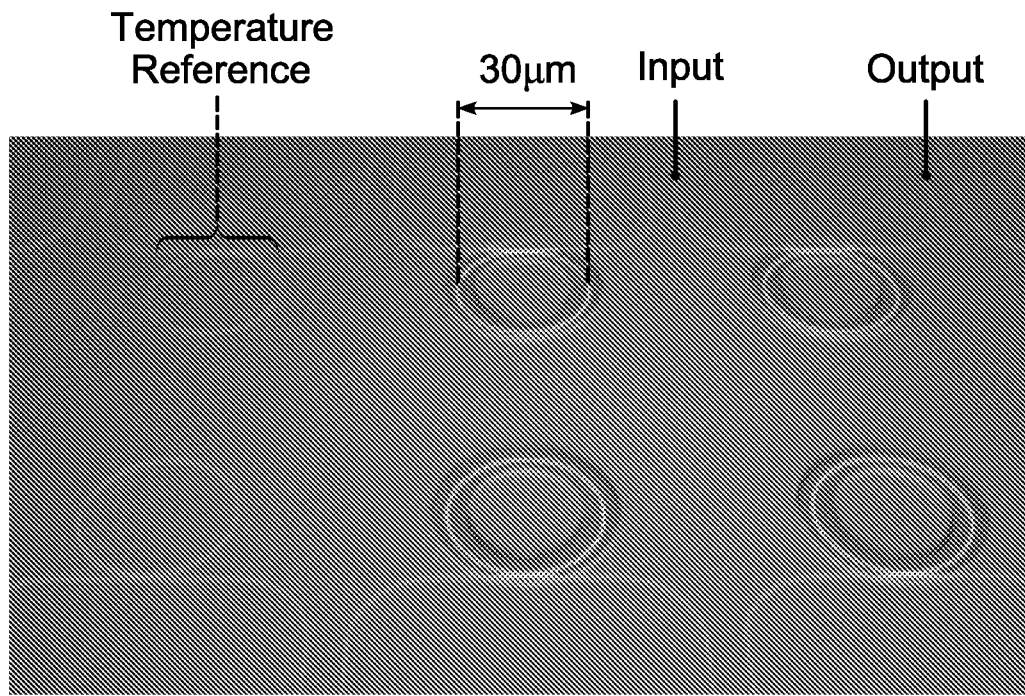


Fig.1C.

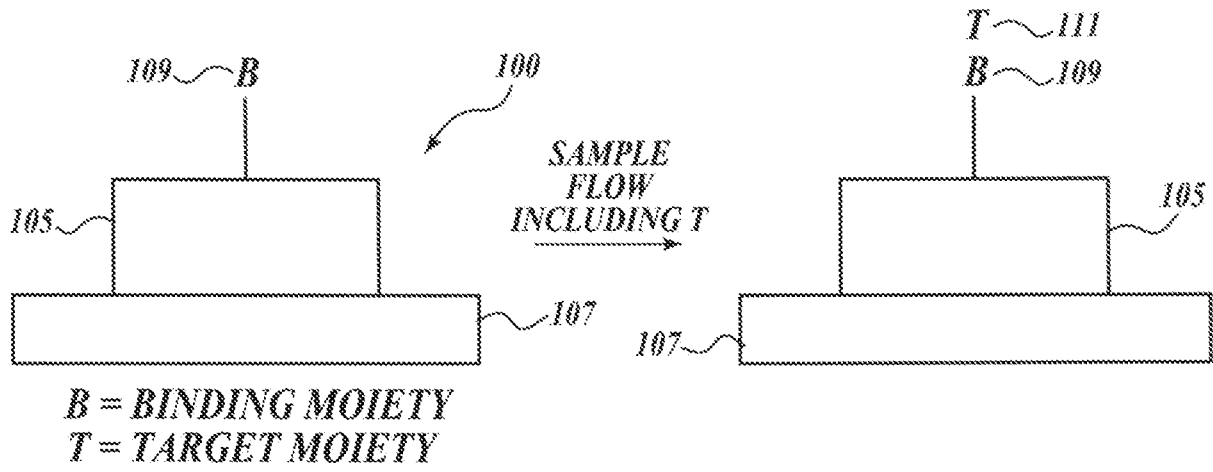


Fig. 1D.

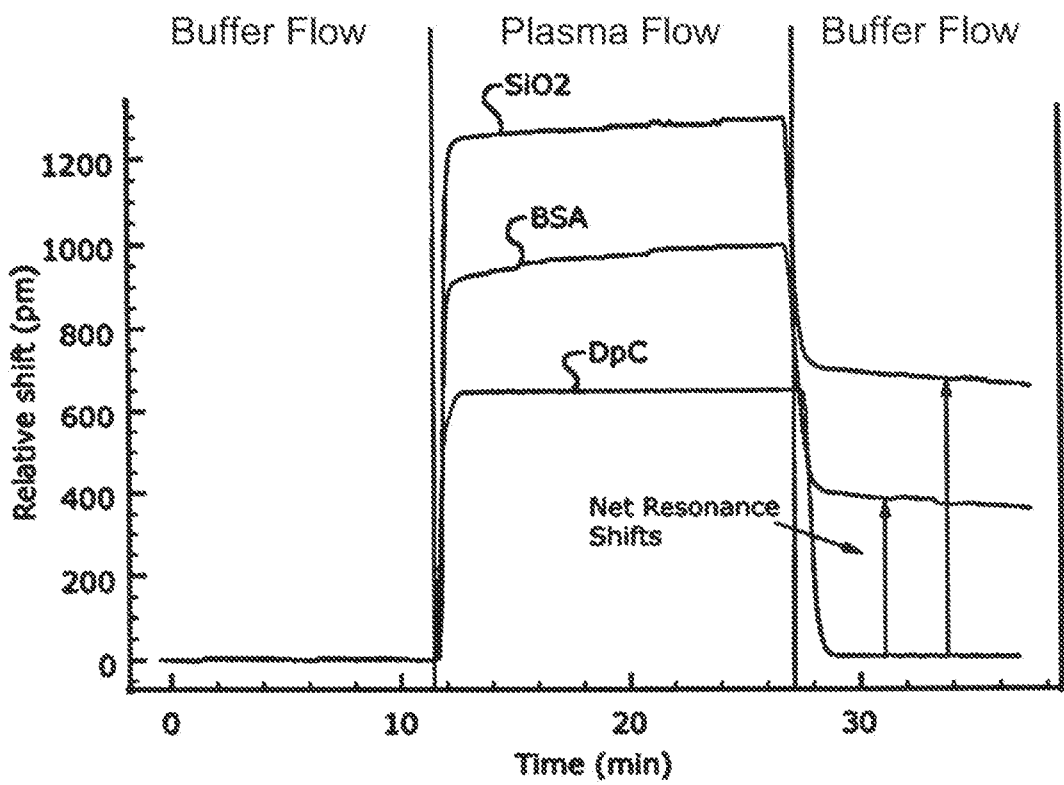


Fig. 2.

5/21

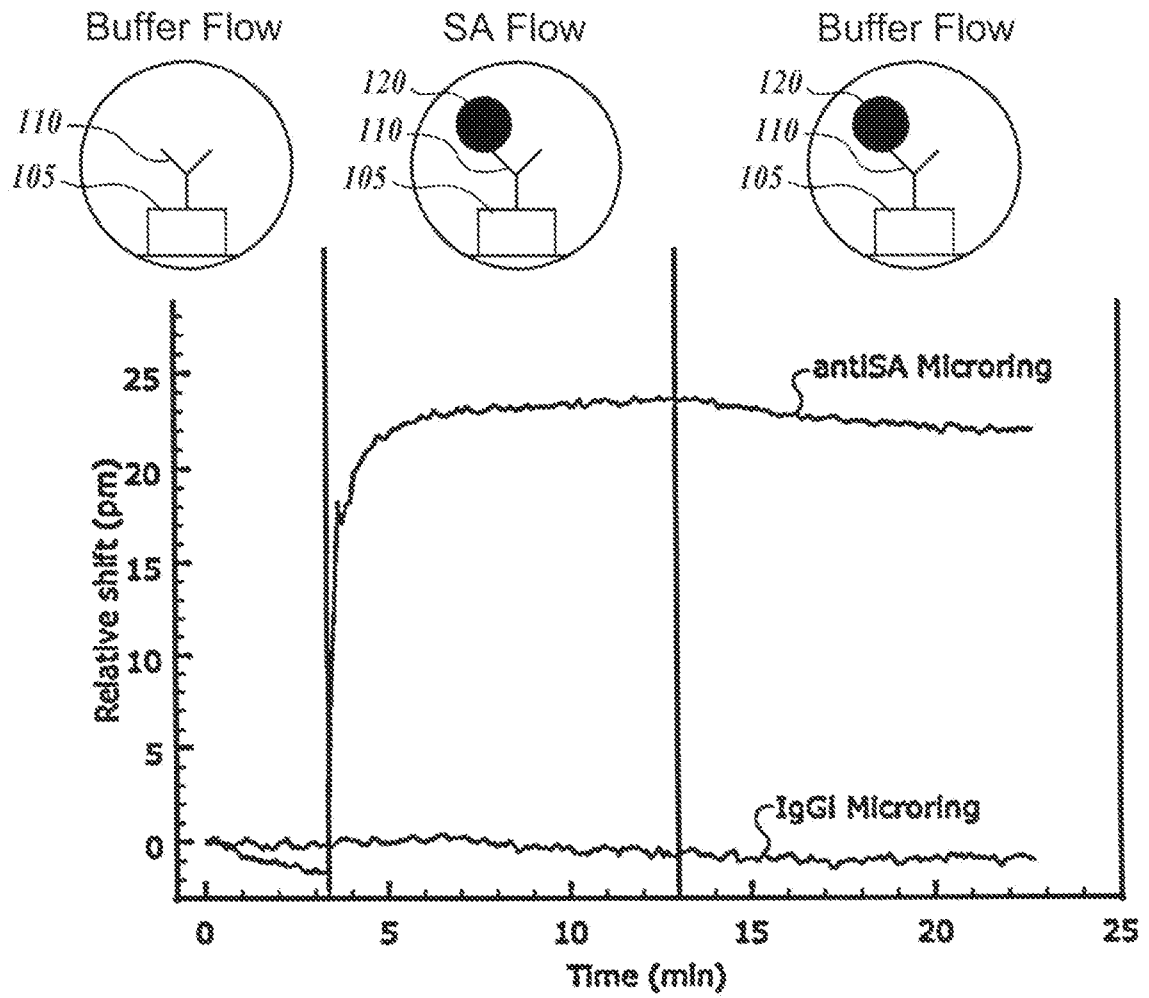


Fig. 3A.

6/21

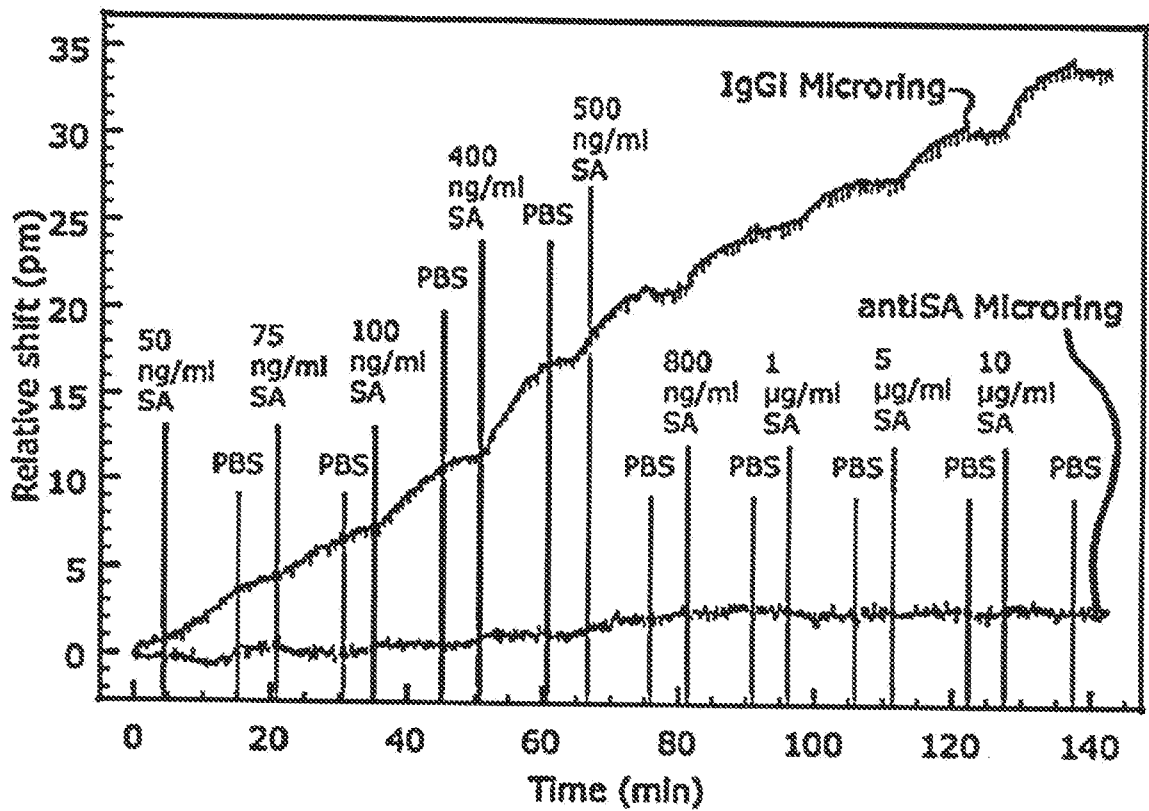


Fig. 3B.

7/21

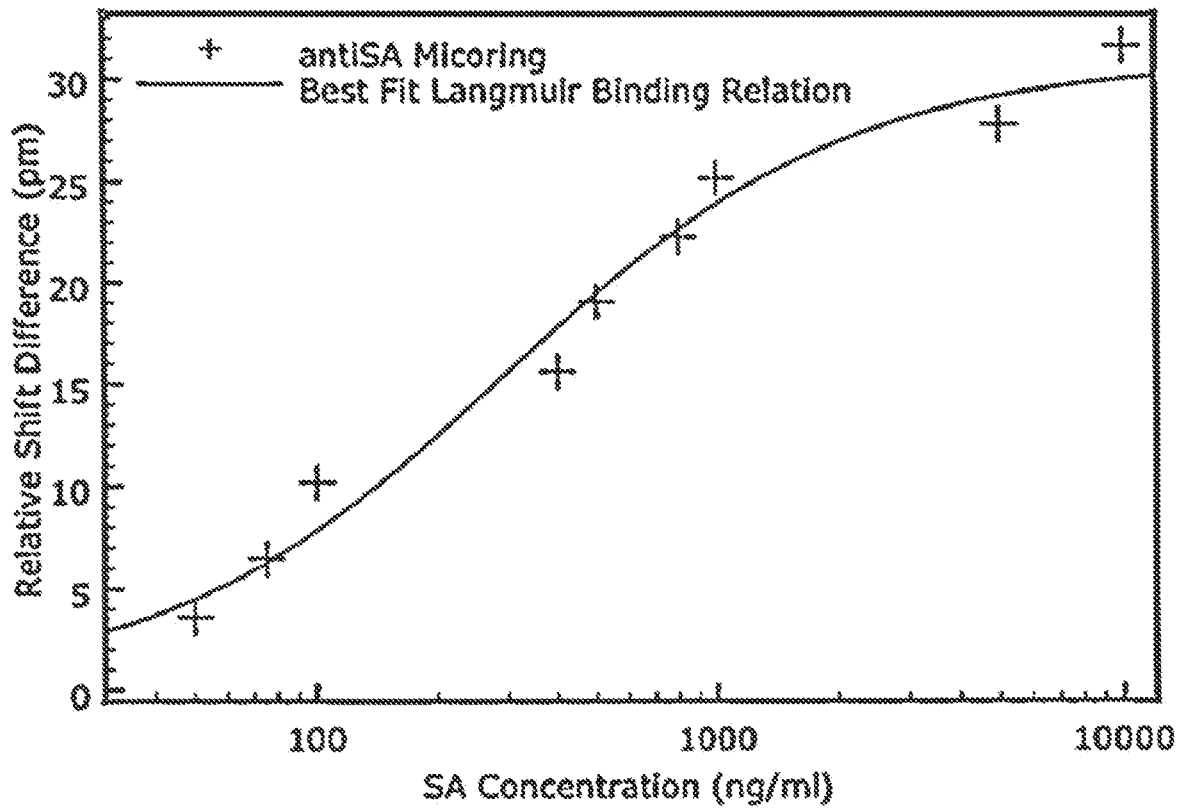


Fig.3C.

8/21

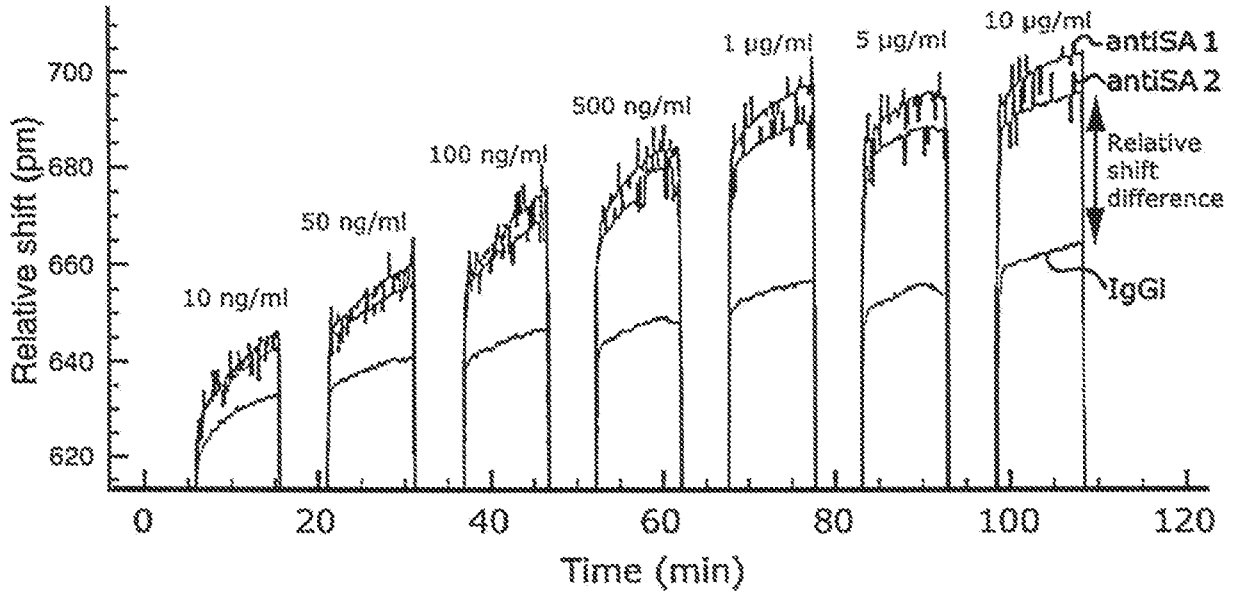


Fig. 4A.

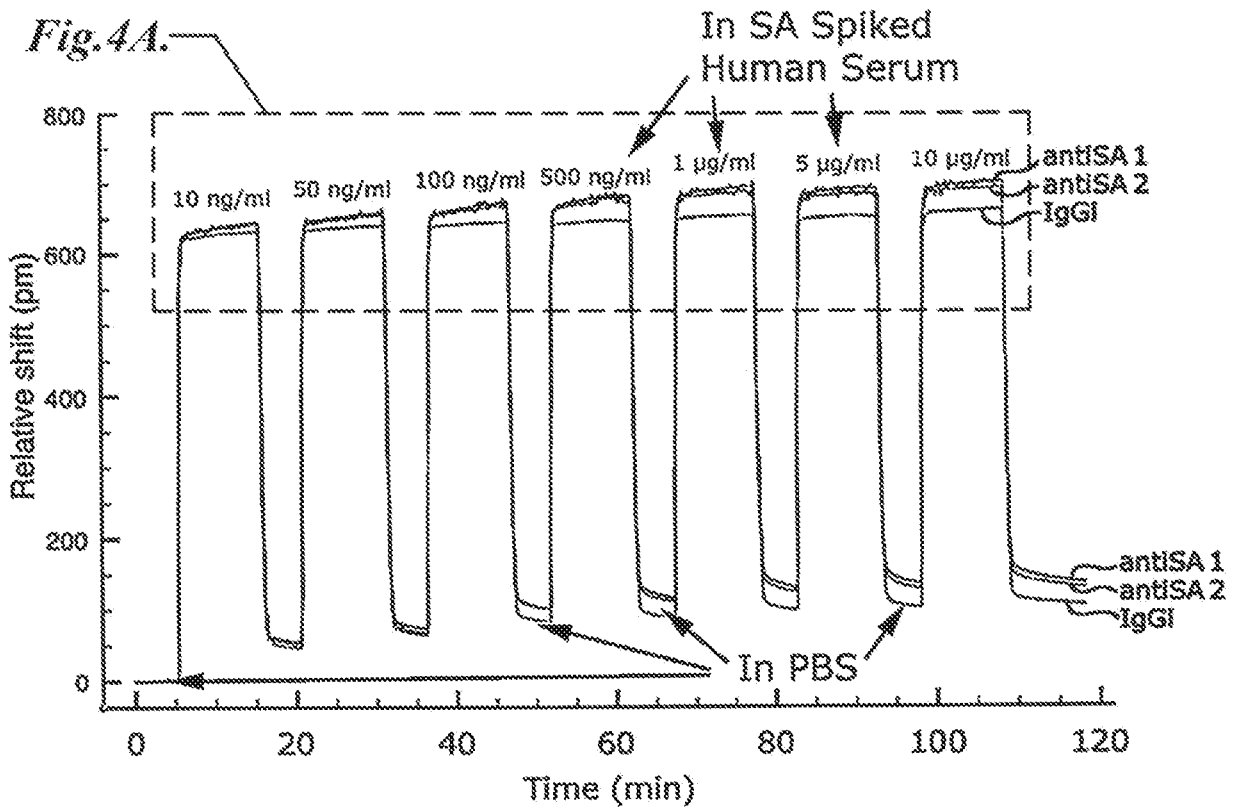


Fig. 4B.

9/21

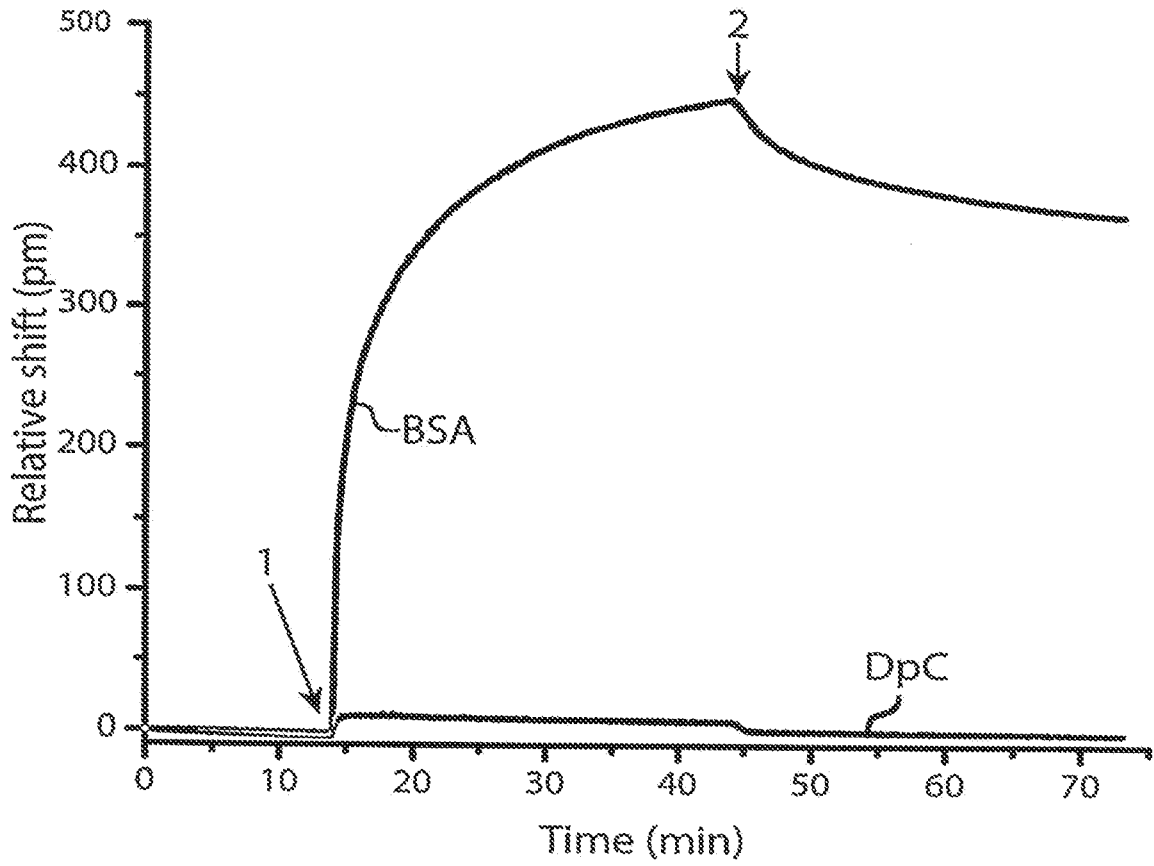


Fig.5.

10/21

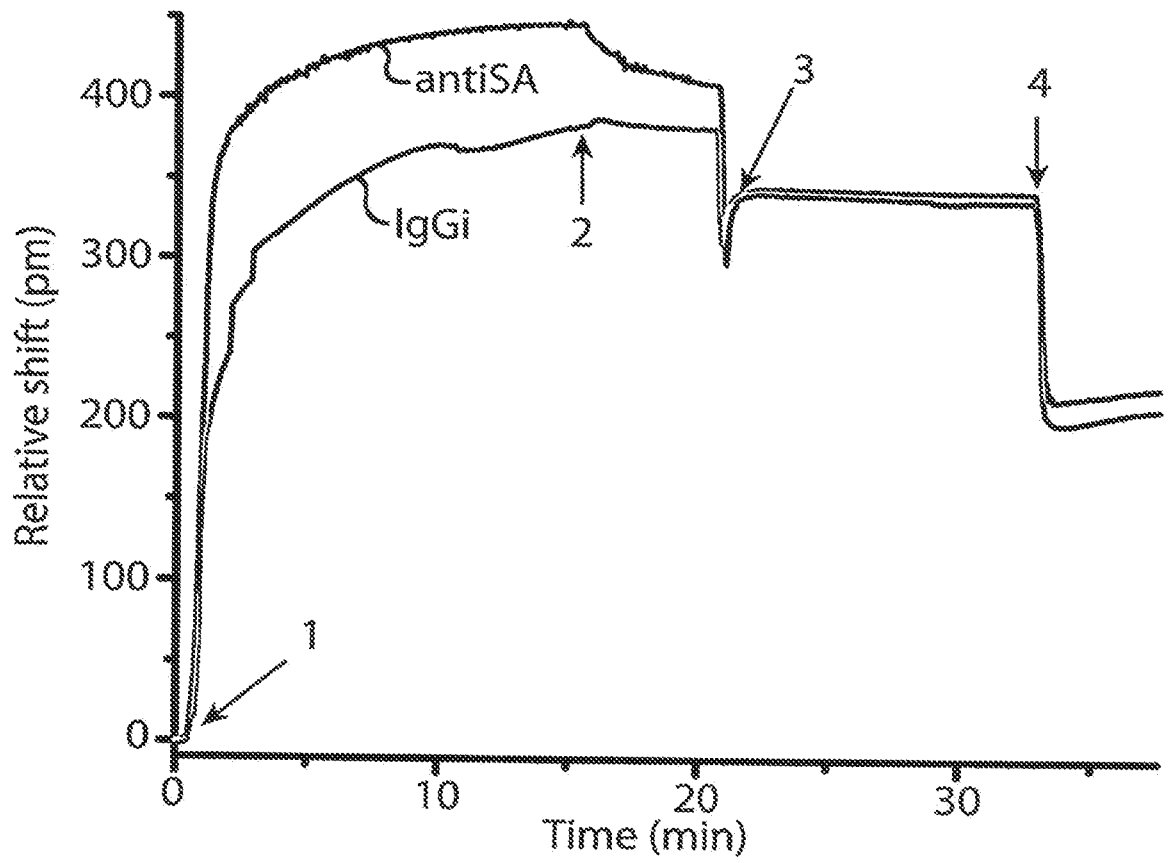
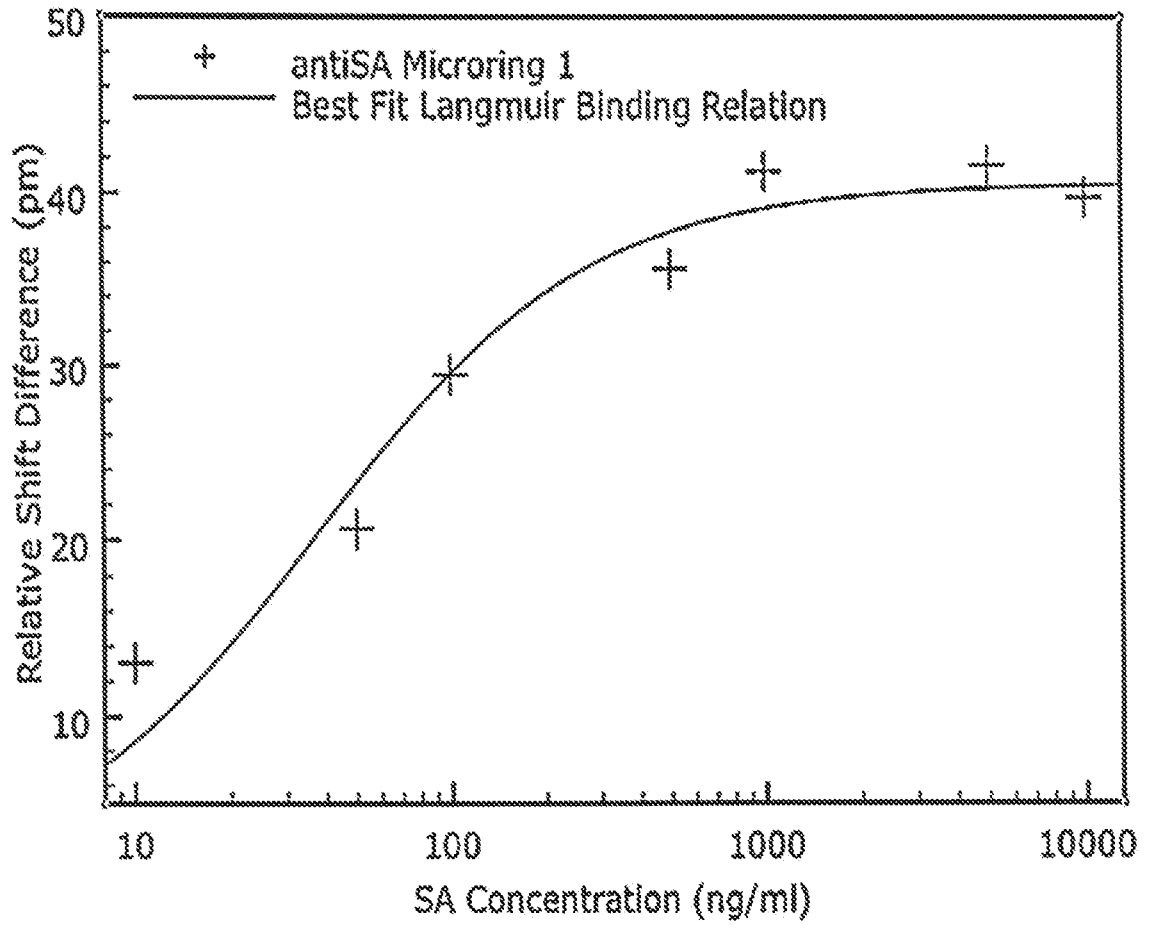
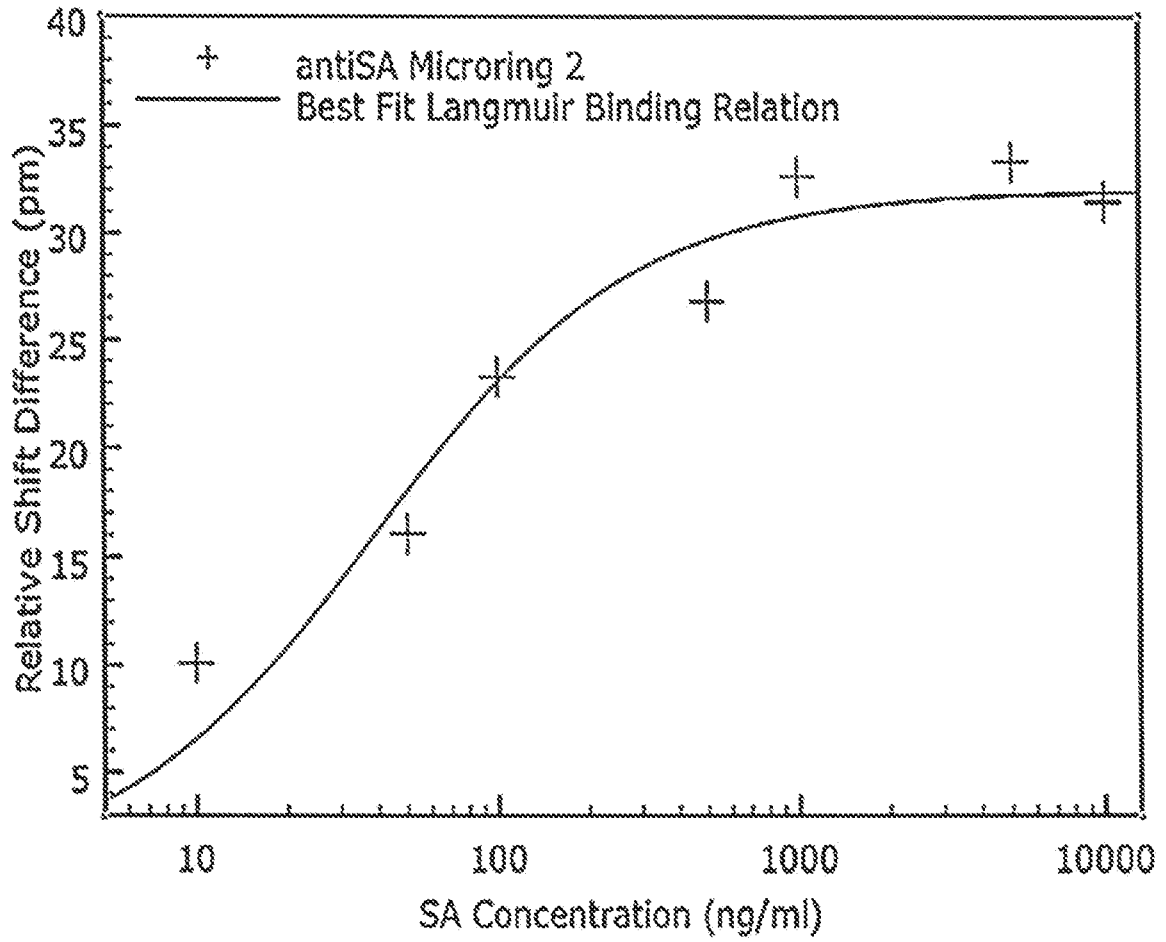


Fig. 6.

11/21

*Fig. 7A.*

12/21

*Fig. 7B.*

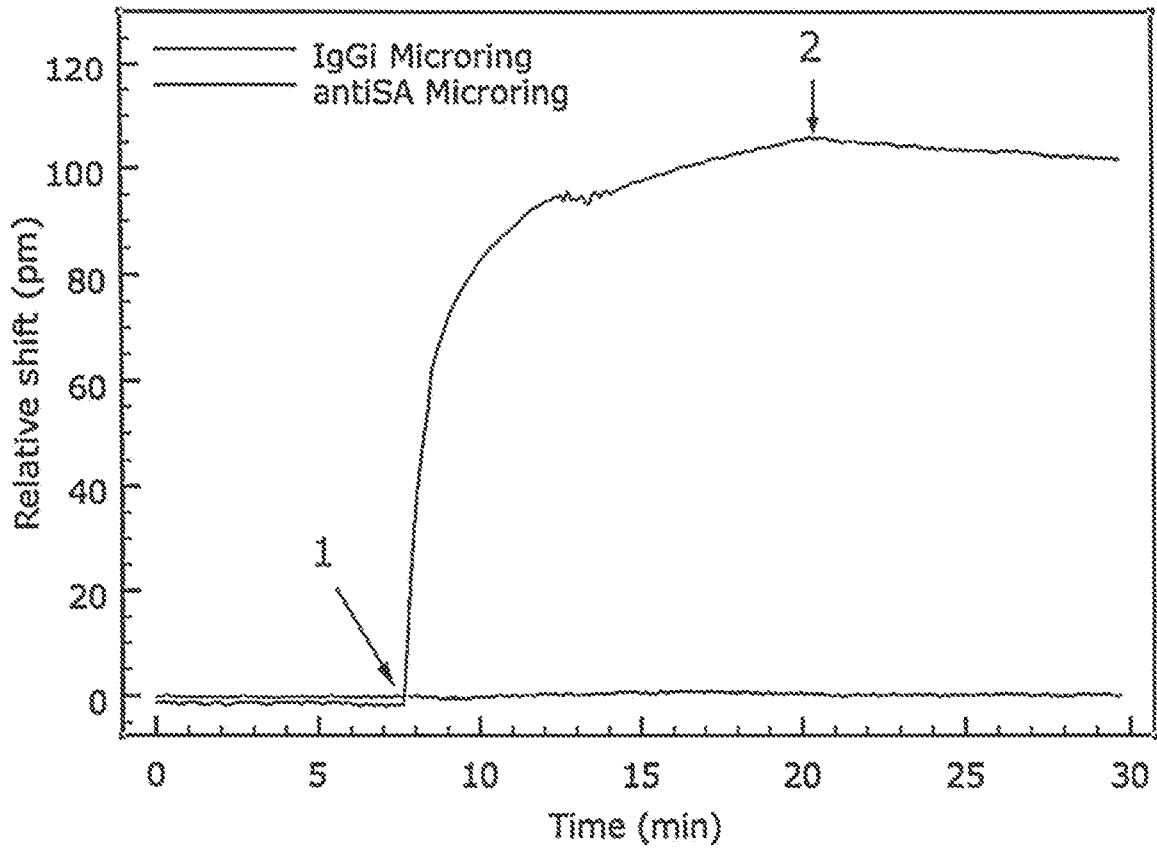


Fig. 8.

Construction of Hierarchical Binding Platform

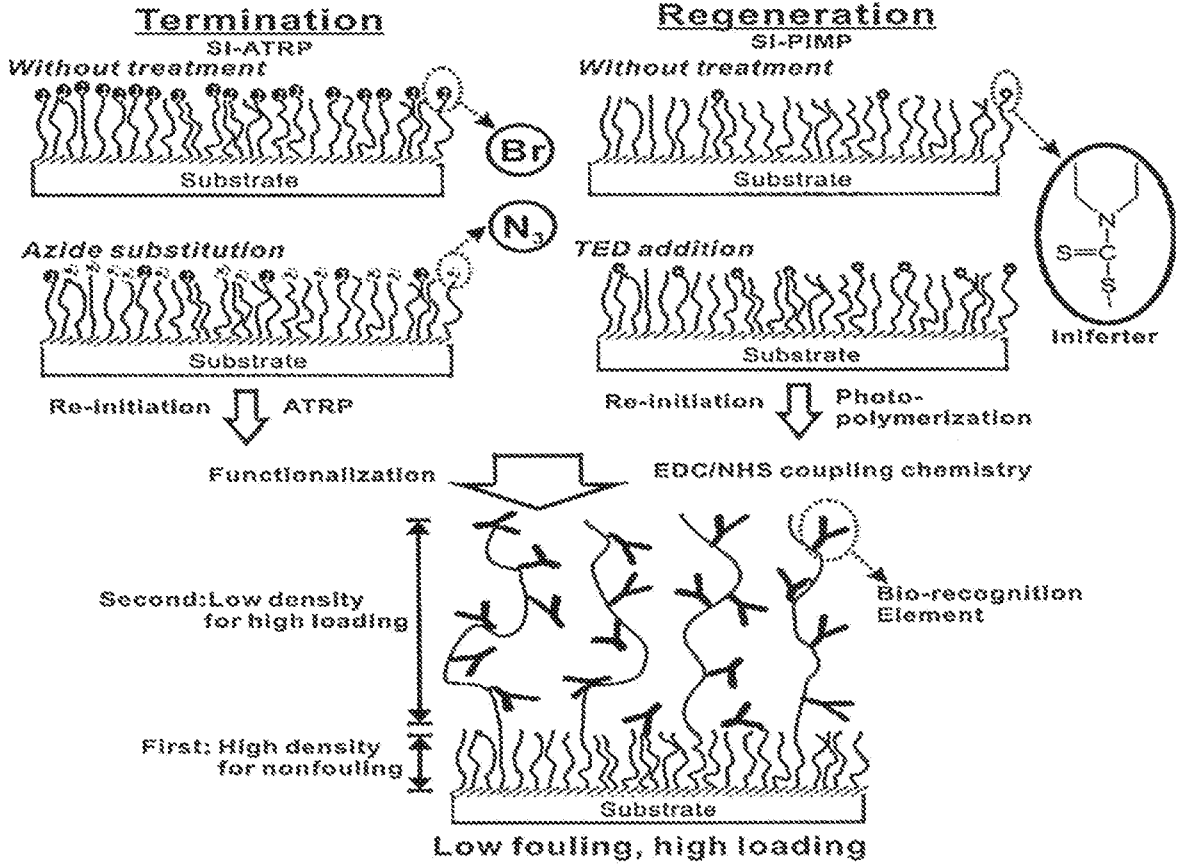


Fig. 9.

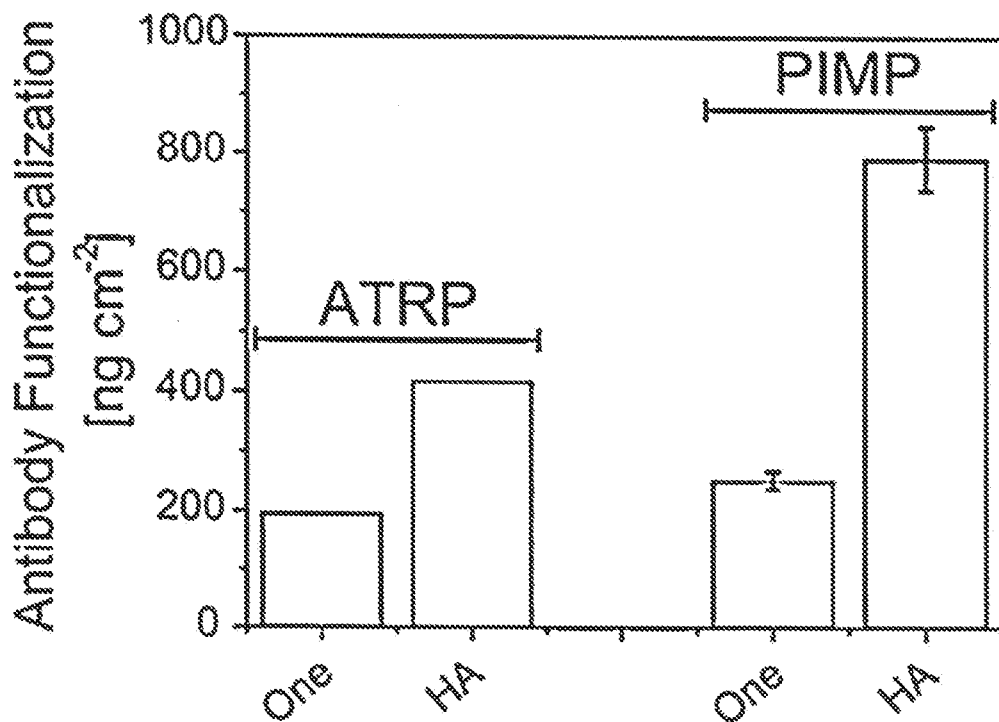


Fig. 10A.

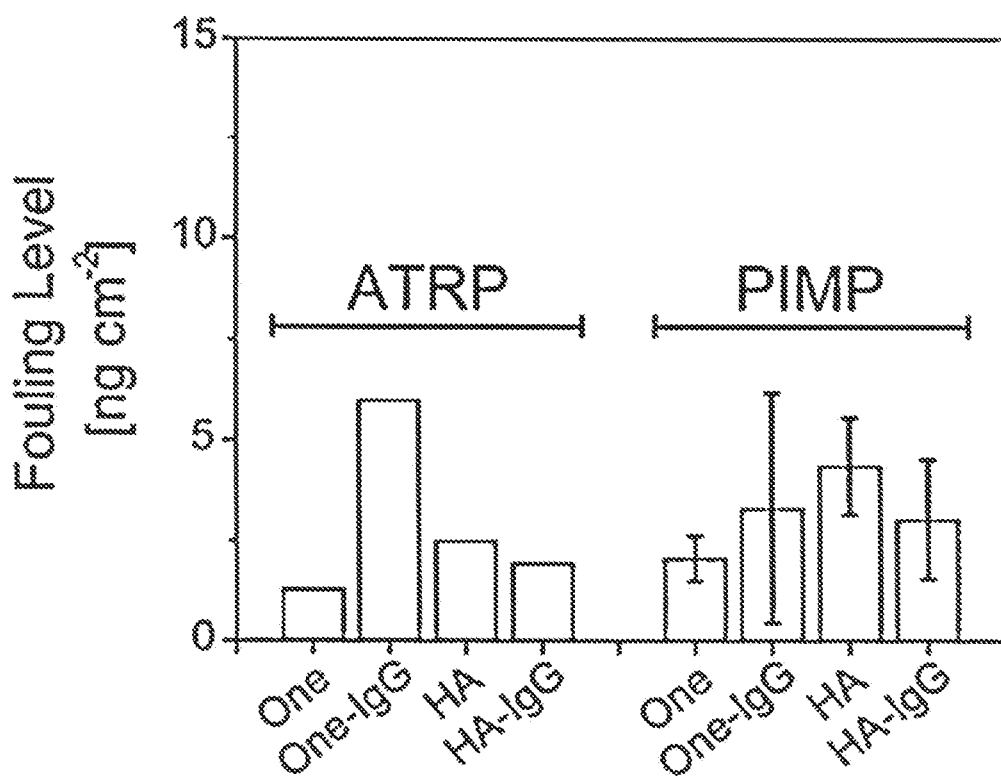


Fig. 10B.

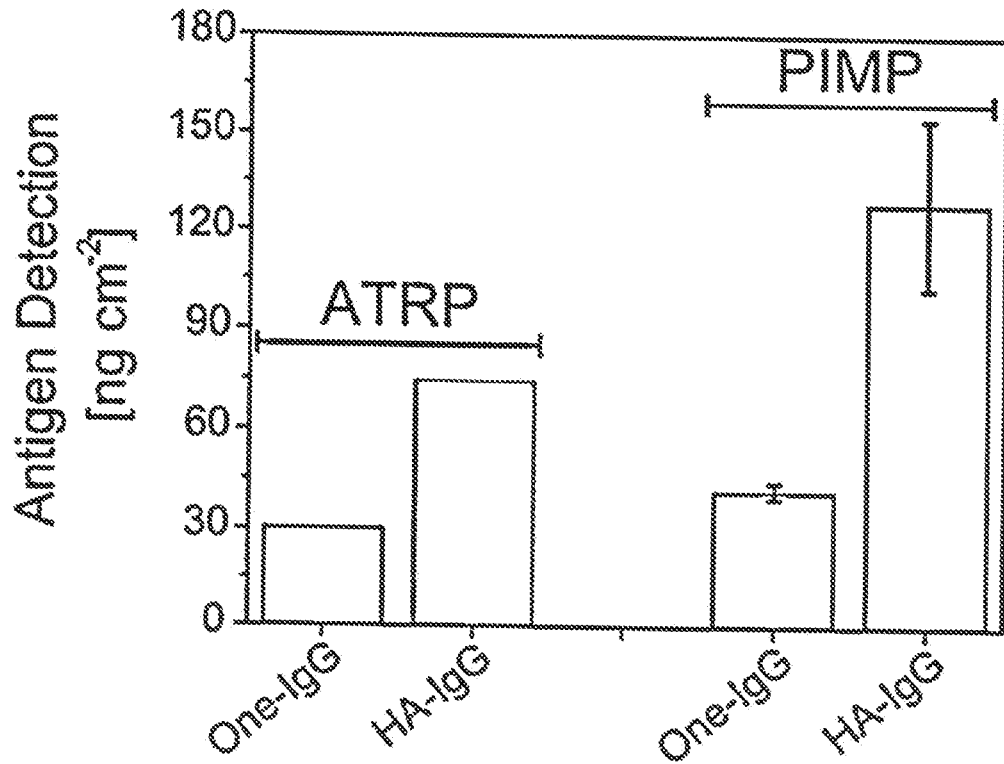


Fig.10C.

17/21

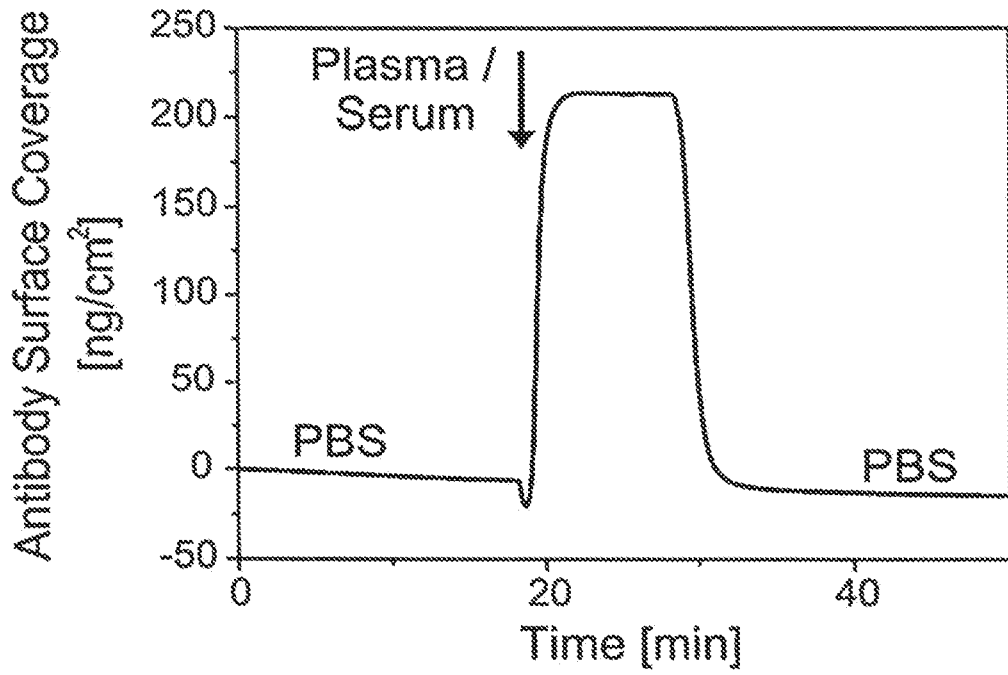


Fig.11.

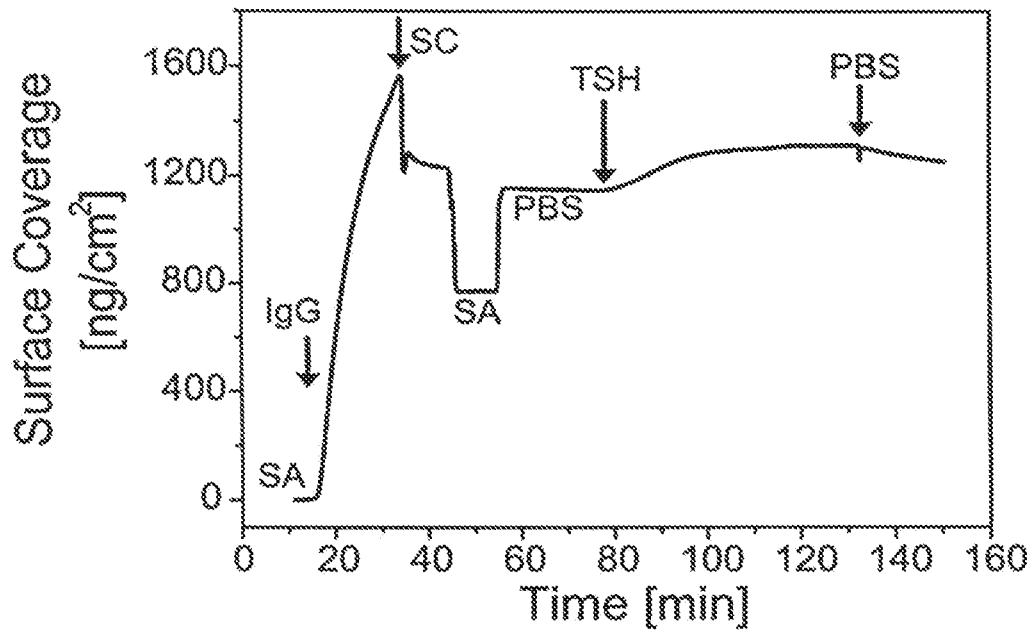


Fig.12.

18/21

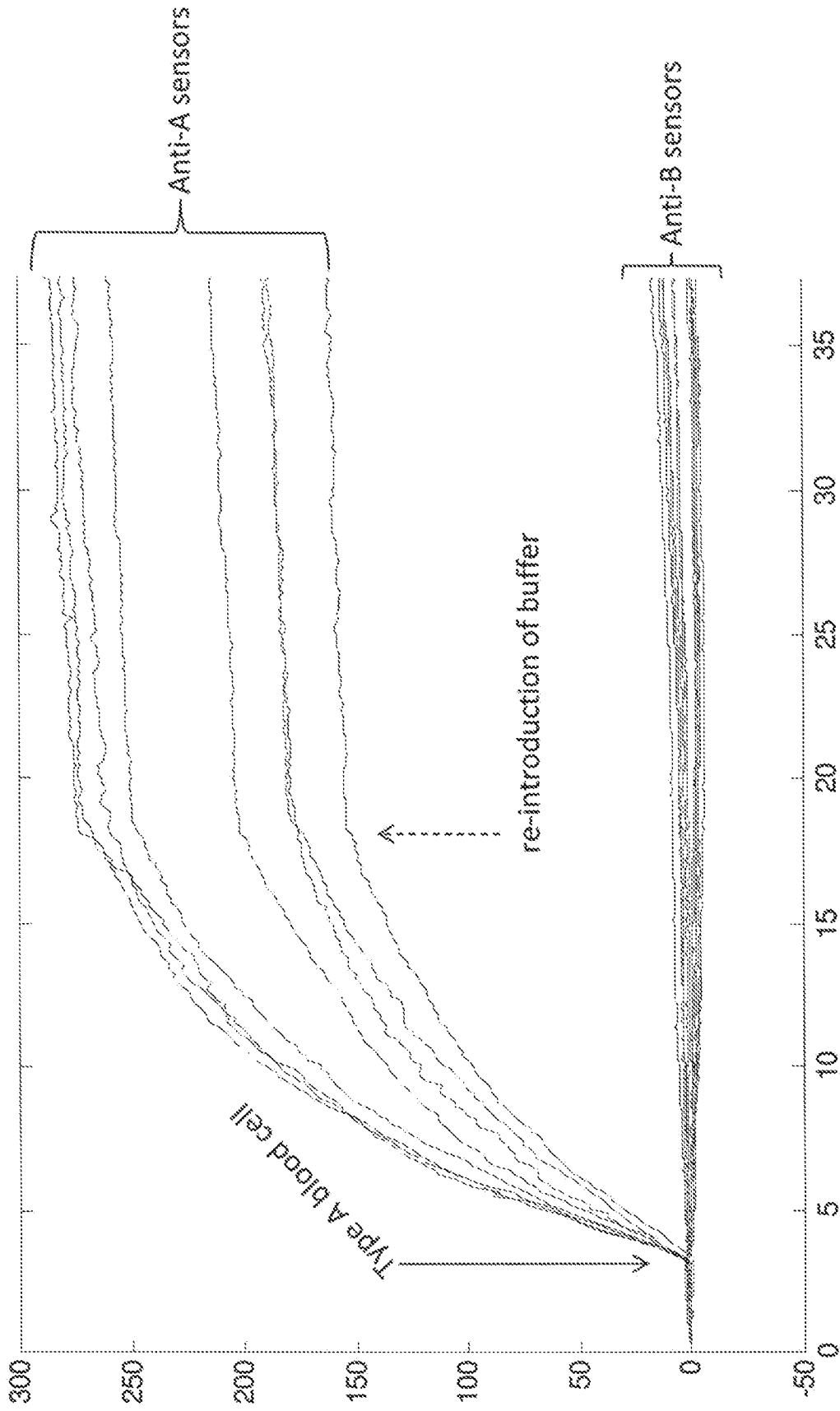


Fig. 13.

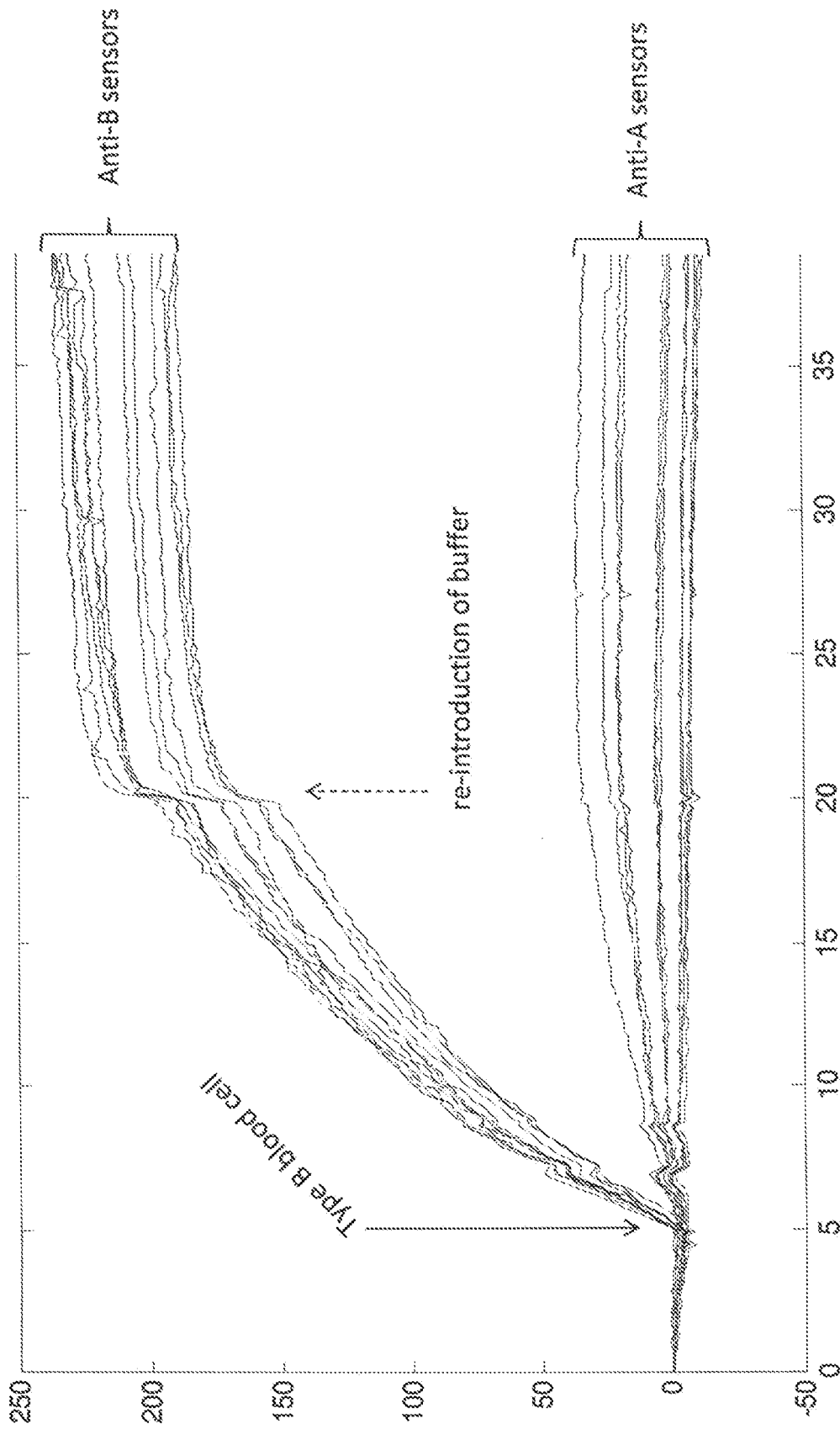


Fig. 14.

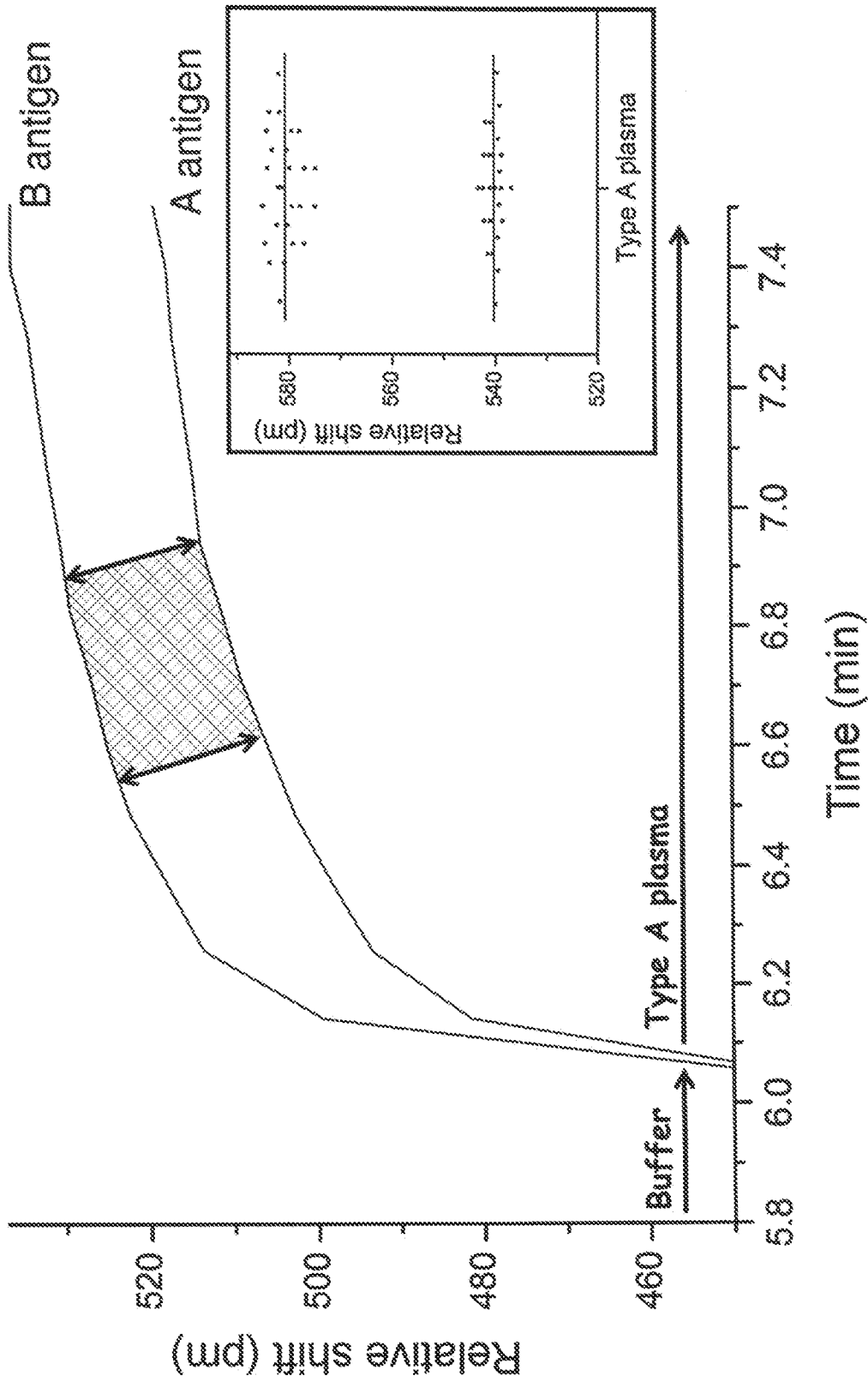


Fig. 15.

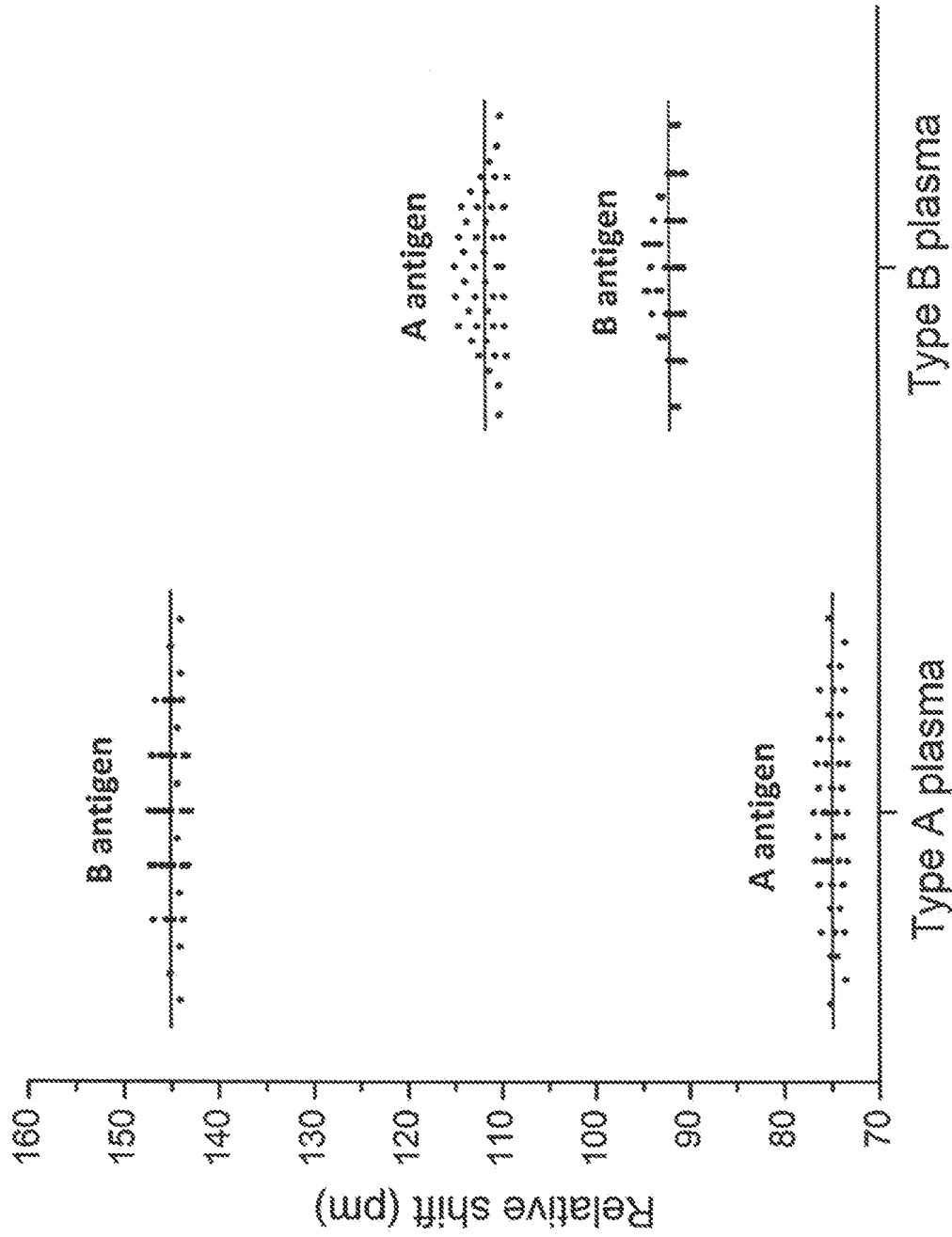


Fig. 16.

专利名称(译)	光子血型		
公开(公告)号	EP2734841A2	公开(公告)日	2014-05-28
申请号	EP2012814998	申请日	2012-07-20
[标]申请(专利权)人(译)	华盛顿大学 普吉特海湾血液CENT 江shaoyl		
申请(专利权)人(译)	华盛顿大学通过其商业中心 普吉特海湾血液中心 江 , shaoyl		
当前申请(专利权)人(译)	华盛顿通过其中心的CO大学 普吉特海湾血液中心		
[标]发明人	BRAULT NORMAN D JIANG SHAOYI RATNER DANIEL M JOHNSEN JILL M KIRK JAMES T LOPEZ JOSE A		
发明人	BRAULT, NORMAN, D. JIANG, SHAOYI RATNER, DANIEL, M. JOHNSEN, JILL, M. KIRK, JAMES, T. LOPEZ, JOSE, A.		
IPC分类号	G01N33/52 G01N33/53 G01N33/80 G01N33/543		
CPC分类号	G01N33/80 G01N21/75 G01N21/7703 G01N33/54373		
优先权	61/588785 2012-01-20 US 61/509776 2011-07-20 US		
其他公开文献	EP2734841A4 EP2734841B1		
外部链接	Espacenet		

摘要(译)

提供了用于检测生物溶液(例如全血)中的分析物的光子装置,系统和方法。代表性的光子器件是具有纳米级特征和微米级直径的光学环谐振器。由于这些装置的紧凑尺寸,许多谐振器可以设置在单个基板上,并且当样品通过装置时同时进行测试。典型的分析物包括血细胞,抗体和病原体,以及指示血细胞或病原体存在的化合物(例如血清学)。在某些实施方案中,血型可以通过使用血细胞的直接检测和血清学的组合的光子传感来确定。通过组合多个装置的检测信号,可以确定血液的类型。

